

# Earth and Space Science



## RESEARCH ARTICLE

10.1029/2021EA002172

## Callisto's Atmosphere and Its Space Environment: Prospects for the Particle Environment Package on Board JUICE

### Key Points:

- Particle Environment Package (PEP) on Jupiter ICy moons Explorer (JUICE) will provide in situ and remote measurements of Callisto's atmosphere and its space environment during ~20 flybys
- We investigate operation plans and instrument capabilities to optimize science return from PEP observations
- The interactions of the atmosphere with the space environment and surface are complex and must be further analyzed in preparation for JUICE

A. Galli<sup>1</sup> , A. Vorburger<sup>1</sup>, S. R. Carberry Mogan<sup>1,2</sup>, E. Roussos<sup>3</sup> , G. Stenberg Wieser<sup>4</sup> , P. Wurz<sup>1</sup> , M. Föhn<sup>1</sup>, N. Krupp<sup>3</sup> , M. Fränz<sup>3</sup>, S. Barabash<sup>4</sup>, Y. Futaana<sup>4</sup> , P. C. Brandt<sup>5</sup>, P. Kollmann<sup>5</sup> , D. K. Haggerty<sup>5</sup> , G. H. Jones<sup>6</sup> , R. E. Johnson<sup>7</sup>, O. J. Tucker<sup>8</sup> , S. Simon<sup>9</sup> , T. Tippens<sup>9</sup>, and L. Liuzzo<sup>10</sup> 

<sup>1</sup>University of Bern, Bern, Switzerland, <sup>2</sup>Center for Space Science, NYU Abu Dhabi, Abu Dhabi, UAE, <sup>3</sup>Max Planck Institute for Solar System Research, Göttingen, Germany, <sup>4</sup>Swedish Institute of Space Physics, Kiruna, Sweden, <sup>5</sup>Johns Hopkins University, Baltimore, MD, USA, <sup>6</sup>Mullard Space Science Laboratory, University College London, London, UK, <sup>7</sup>University of Virginia, Charlottesville, VA, USA, <sup>8</sup>NASA Goddard Space Flight Center, Greenbelt, MD, USA, <sup>9</sup>School of Earth & Atmospheric Sciences, Georgia Institute of Technology, Atlanta, GA, USA, <sup>10</sup>Space Sciences Laboratory, University of California, Berkeley, CA, USA

### Correspondence to:

A. Galli,  
[andre.galli@space.unibe.ch](mailto:andre.galli@space.unibe.ch)

### Citation:

Galli, A., Vorburger, A., Carberry Mogan, S. R., Roussos, E., Stenberg Wieser, G., Wurz, P., et al. (2022). Callisto's atmosphere and its space environment: Prospects for the Particle Environment Package on board JUICE. *Earth and Space Science*, 9, e2021EA002172. <https://doi.org/10.1029/2021EA002172>

Received 14 DEC 2021

Accepted 20 APR 2022

### Author Contributions:

**Conceptualization:** A. Galli

**Formal analysis:** A. Vorburger

**Investigation:** A. Galli, A. Vorburger, S. R. Carberry Mogan, E. Roussos, G. Stenberg Wieser, Y. Futaana, R. E. Johnson, S. Simon, T. Tippens, L. Liuzzo

**Methodology:** A. Galli, A. Vorburger, S. R. Carberry Mogan, E. Roussos, G. Stenberg Wieser, T. Tippens, L. Liuzzo

**Project Administration:** A. Galli

**Resources:** S. Barabash

**Supervision:** A. Galli

**Validation:** A. Galli, S. R. Carberry Mogan, E. Roussos, G. Stenberg Wieser, P. Wurz, M. Föhn, N. Krupp, M. Fränz, S. Barabash, Y. Futaana, P. C. Brandt, P.

**Abstract** The Jupiter ICy moons Explorer (JUICE) of the European Space Agency will investigate Jupiter and its icy moons Europa, Ganymede, and Callisto, with the aim to better understand the origin and evolution of our Solar System and the emergence of habitable worlds around gas giants. The Particle Environment Package (PEP) on board JUICE is designed to measure neutrals and ions and electrons at thermal, suprathermal, and radiation belt energies (eV to MeV). In the vicinity of Callisto, PEP will characterize the plasma environment, the outer parts of Callisto's atmosphere and ionosphere and their interaction with Jupiter's dynamic magnetosphere. Roughly 20 Callisto flybys with closest approaches between 200 and 5,000 km altitude are planned over the course of the JUICE mission. In this article, we review the state of the art regarding Callisto's ambient environment and magnetospheric interaction with recent modeling efforts for Callisto's atmosphere and ionosphere. Based on this review, we identify science opportunities for the PEP observations to optimize scientific insight gained from the foreseen JUICE flybys. These considerations will inform both science operation planning of PEP and JUICE and they will guide future model development for Callisto's atmosphere, ionosphere, and their interaction with the plasma environment.

## 1. Introduction

Callisto is often perceived as a boring and archaic satellite when compared to its seemingly more exciting neighbors: Io is the most volcanically active body in the solar system (Lopes, 2014 and references therein), Europa harbors a global subsurface ocean with features conducive to biology (Hand et al., 2009 and references therein), and Ganymede is the only known satellite in the solar system to possess an intrinsic magnetic field (Kivelson et al., 1996). Moreover, Io and Europa have extremely young surfaces, and Ganymede has many diverse terrains and landforms. In contrast, images of Callisto taken during Voyager flybys revealed a surface sculpted by impacts, making it the most heavily cratered Galilean satellite (Smith, Soderblom, Johnson, et al., 1979; Smith, Soderblom, Beebe, et al., 1979) and one of the oldest surfaces in the solar system. This implied that Callisto's surface was devoid of any active endogenic processes. The stigma of Callisto being an old, frozen, and geologically dead moon persisted until Galileo revealed that it is home to several exciting processes and yet unresolved mysteries of its own. For example, high-resolution images of Callisto taken by Galileo showed a surprisingly near absence of small craters on the surface, implying that, contrary to the aforementioned assumptions made about Callisto's endogenic activity, small crater degradation processes are occurring (Moore et al., 1999). Moore et al. (1999) demonstrated that these features were a result of sublimation-driven landform modification and mass wasting, and suggested Callisto possessed the most degraded surface of the icy Galilean satellites. A recent investigation by Stephan et al. (2020) of the size-distribution of water ice particles on the surface underlined the importance of temperature-driven processes for the physical properties of Callisto's surface, similar to its inner neighbor Ganymede.

Although Callisto and Ganymede are of similar size and bulk composition, there are several dichotomies between the two bodies that make for an interesting comparison. While the surface of Ganymede features more diverse and complex terrains (Schenk, 1995), the surface of Callisto, in addition to being the oldest and most heavily

© 2022 The Authors.

This is an open access article under the terms of the [Creative Commons Attribution-NonCommercial License](https://creativecommons.org/licenses/by-nc/4.0/), which permits use, distribution and reproduction in any medium, provided the original work is properly cited and is not used for commercial purposes.

Kollmann, D. K. Haggerty, G. H. Jones, R. E. Johnson, O. J. Tucker, S. Simon, T. Tippens, L. Liuzzo  
**Visualization:** A. Galli, S. R. Carberry Mogan, E. Roussos, S. Simon  
**Writing – original draft:** A. Galli  
**Writing – review & editing:** A. Galli, A. Vorburger, S. R. Carberry Mogan, E. Roussos, G. Stenberg Wieser, P. Wurz, M. Föhn, N. Krupp, M. Fränz, S. Barabash, Y. Futaana, P. C. Brandt, P. Kollmann, R. E. Johnson, O. J. Tucker, S. Simon, T. Tippens, L. Liuzzo

cratered of those of the Galilean satellites, was observed by Galileo to also have the most degraded surface (Moore et al., 1999). In addition to such geomorphological differences, each body has had a radically different evolutionary path. For example, Ganymede was discovered to possess an intrinsic magnetic field (Kivelson et al., 1996); however, plasma wave and magnetometer observations of Callisto indicated that it does not have an intrinsic magnetosphere or internal magnetic field (Gurnett et al., 1997; Khurana et al., 1997). This was consistent with the measurements of Callisto's gravitational field which implied the moon was only partially differentiated and consisted of a homogeneous mixture of roughly ~50% (by mass) compressed ice and ~50% rock (Anderson et al., 1997; Kuskov & Kronrod, 2005; Spohn & Schubert, 2003).

The incomplete differentiation of Callisto's interior may be due to the lack of strong tidal heating. Whereas the orbital paths of the three innermost Galilean satellites are influenced by strong Laplace resonances, Callisto only experiences a weak (3:7) resonance with Ganymede (Celletti et al., 2021; Rambaux et al., 2011). Moreover, Callisto as the outermost of the four Galilean moons is 26.3 Jupiter radii away from Jupiter. As a consequence, Callisto encountered less tidal heating over its history (Musotto et al., 2002), albeit its rotation is tidally locked with Jupiter. Magnetic field perturbations measured by Galileo imply that Callisto, like Europa and possibly also Ganymede, possesses an interior salty liquid-water ocean (Khurana et al., 1998). The magnetic field measurements were consistent with dipole fields induced by the temporal variations of the ambient Jovian magnetic field (Zimmer et al., 2000). Since Callisto is known to have an icy and thus nonconducting surface, a global subsurface ocean has been suggested to be the conducting medium (e.g., see Zimmer et al., 2000 and references therein). The postulation of a subsurface ocean on Callisto, which shows few signs of differentiation, is indeed a baffling one and must be investigated further (Grasset et al., 2013). The existence of Callisto's ocean is also the most disputed among the three outer Galilean moons, because Callisto is surrounded by a dense, asymmetric and variable ionosphere which may also drive induced fields.

In addition, Callisto orbits in one of the most dynamic regions of Jupiter's magnetosphere, and is exposed to a variety of plasma environments, exposing the moon to a multitude of space plasma interaction modes. All things considered, Callisto constitutes a unique exploration target, both from the perspective of planetary geology and habitability and from that of fundamental space plasma physics.

The JUPITER ICy moons Explorer (JUICE) of the European Space Agency will investigate the icy moons of Jupiter, the Jovian space environment, and their interactions. JUICE is scheduled for launch in 2023 and will perform several flybys at Europa, Ganymede, and Callisto from 2031 unto 2034 before entering into orbit around Ganymede by the end of 2034. The science objectives of JUICE for Callisto “as a remnant of the early Jovian system” are threefold (Grasset et al., 2013; Hussmann et al., 2014):

- (1) Characterize the structure of the outer icy shell including the possible detection of shallow subsurface water; determine the extent of the subsurface ocean (if it exists) and its main physicochemical properties
- (2) Characterize the composition and chemistry of Callisto's surface, in particular for nonwater-ice compounds. Provide a consistent picture of the surface chemistry and separate the relative contributions of endogenic subsurface chemistry and exogenic magnetosphere-driven radiolysis and sputtering. Reveal information about the sources and sinks of the atmosphere to constrain the origin and evolution of Callisto's volatile inventory. Also characterize the ionospheric composition, structure, and dynamics
- (3) Investigate the unique erosion and degradation processes on Callisto's densely cratered plains. Improve our understanding of the geologic evolution of Callisto by constraining its surface ages. Verify whether hydrostatic equilibrium is actually obtained and improve our understanding of the degree of differentiation of Callisto's interior

To achieve the first two objectives, the space plasma environment, the atmosphere, and the ionosphere of Callisto must be investigated in detail. The atmosphere and ionosphere are the links between the surface and the space environment and they are the only regions where surface material from Callisto (released by sputtering, sublimation, and other surface interaction processes) can be measured in situ during flybys. In addition, the magnetic induction response from Callisto is crucial to better constrain Callisto's interior and to learn more about its putative salt water ocean. For all these reasons, the measurements with the Particle Environment Package (PEP) during JUICE flybys will be indispensable for achieving the first two science objectives. The corresponding science questions for PEP can be grouped into two categories: (A) What is the chemical composition and the three-dimensional distribution of Callisto's atmosphere and ionosphere and how do they depend on the space

environment (illumination, magnetic field configuration, local plasma properties, etc.)? (B) Provided the space environment in the absence of Callisto's influence is adequately characterized, how does Callisto affect its space environment via for example, mass loading, induced magnetic fields, plasma wake, and formation of a neutral torus?

This paper is organized as follows: in Section 2 we first summarize the present knowledge on Callisto's atmosphere and its space environment. Section 3 then explains in more detail the JUICE mission, its trajectory and the PEP instruments. Section 4 summarizes the PEP observation opportunities related to science questions A (neutral atmosphere, neutral torus, and generation of Energetic Neutral Atoms (ENA) in Sections 4.1 – Sections 4.3 and B (ENAs and charged particle environment in Sections 4.3 and 4.4). These considerations lead to recommendations for PEP operation planning and for modeling work over the next decade until the advent of JUICE (Section 5). Section 6 concludes the paper.

## 2. Callisto's Atmosphere and Its Space Environment

### 2.1. Callisto's Atmosphere

Callisto's atmosphere is poorly constrained, and its origin and evolution are not well understood. A tenuous CO<sub>2</sub> atmosphere was observed by Galileo, and Carlson (1999) suggested that its extent was global due to the volatility and mobility of CO<sub>2</sub> at Callisto's surface temperatures. Galileo radio occultations also indicated the presence of a sometimes substantial but also highly variable ionosphere, which was suggested to originate from an inferred O<sub>2</sub> atmosphere (Kliore et al., 2002), about two orders of magnitude denser than that of the observed CO<sub>2</sub>. UV auroral emissions were not detected in subsequent Hubble Space Telescope (HST)-Space Telescope Imaging Spectrograph (STIS) observations, which was suggested to be due to Callisto's substantial ionosphere diverting the flow of the corotating Jovian thermal electrons, that are expected to drive these UV emissions through collisions with O<sub>2</sub> (Strobel et al., 2002). Despite this nondetection, upper limits for O and C could be estimated. Atomic oxygen emissions detected using the HST-Cosmic Origins Spectrograph were suggested to be induced by photoelectron impacts in an O<sub>2</sub>-dominated atmosphere (Cunningham et al., 2015), with a derived O<sub>2</sub> column density an order of magnitude less than that suggested by Kliore et al. (2002). However, even this reduced estimate for the density of Callisto's atmosphere (column density  $\geq 10^{15}$  cm<sup>-2</sup>) is exceeded among other solar system satellites only by the atmospheres on Io, Triton, and Titan (Cunningham et al., 2015). Faint atmospheric emissions above Callisto's limb were recently detected from HST-Space Telescope Imaging Spectrograph observations (Roth et al., 2017), likely originating from resonant scattering by an H corona. This corona was suggested to be produced via dissociation of sublimated H<sub>2</sub>O and sputtered or radiolytically produced H<sub>2</sub> (e.g., Carberry Mogan et al., 2021) from Callisto's icy surface.

The efforts to model Callisto's atmosphere can be summarized as follows: Liang et al. (2005) applied a range of one-dimensional chemistry models to reproduce the electron densities of Kliore et al. (2002) while satisfying the upper limits of atmospheric densities (Strobel et al., 2002). Liang et al. (2005) accounted for H<sub>2</sub>O, CO<sub>2</sub>, O<sub>2</sub>, and all resulting neutrals and ions formed via reactions and photochemistry in an isothermal atmosphere close to the surface. Since photoionization of the observed CO<sub>2</sub> could not produce the electron densities consistent with Kliore et al. (2002), they also suggested a denser, predominantly O<sub>2</sub> atmosphere to be present. Hartkorn et al. (2017) used a 3D ionosphere model in an O<sub>2</sub>, CO<sub>2</sub>, H<sub>2</sub>O atmosphere with photoionization and collisions between photoelectrons and neutrals as the sources of the ionospheric electrons and the UV emissions. Whereas the CO<sub>2</sub> was assumed to be globally uniform, strong day-night asymmetries were estimated for the O<sub>2</sub> and H<sub>2</sub>O components according to the surface temperature affecting the H<sub>2</sub>O vapor pressure and the production of O<sub>2</sub> by magnetospheric ion-induced sputtering and photochemical reactions. Vorburger et al. (2015) applied a 1D Monte Carlo model to simulate sublimation, sputtering and photodesorption of 34 ice and nonice species in the surface-bound exosphere of Callisto. They explored the parameter space by varying surface composition and temperature as well as atmospheric sources and sinks. Vorburger et al. (2019) improved on this by expanding to 3D and differentiating between cold and hot magnetospheric plasma sputtering of the surface. They also considered the influence of ionospheric shielding by assuming that when an ionosphere was present, only the energetic particles could impact the surface and did so isotropically, otherwise both the cold and hot plasma impacted the surface with the former preferentially impacting the ramside. Carberry Mogan et al. (2020) applied a 1D molecular kinetics model to simulate intermolecular collisions and thermal escape in single and multicomponent atmospheres

on Callisto composed of radiolytically produced volatiles ( $\text{CO}_2$ ,  $\text{O}_2$ ,  $\text{H}_2$ ), which were assumed to permeate the porous regolith and thermally desorb. Applying densities inferred from observations and models, they showed that intermolecular collisions are critical for describing the structure of and escape from Callisto's atmosphere. Carberry Mogan et al. (2021) followed up this work by expanding their model to 2D to include the diurnal variation of Callisto's surface temperature and the corresponding local and global transport, as well as sublimated water vapor. They compared the production of H via photodissociation by sublimated water vapor to that by radiolytically produced  $\text{H}_2$  suggesting the latter is the primary source of the detected H corona near and beyond the terminator because of its roughly global distribution and large-scale height. The previously ignored extended  $\text{H}_2$  component likely has a critical effect on the plasma-neutral interactions at Callisto.

In summary, the different atmosphere models cover most relevant physical processes, but no single model so far includes all relevant processes and species in 3D. Moreover, the models so far are not fully self-consistent: for instance, sputtering contributes to the exosphere formation, which in turn would reduce primary ion irradiation while enhancing secondary ion precipitation. Another potentially important aspect worth being studied in more detail is atmospheric sputtering or plasma-stripping (Johnson, 2004). The denser atmosphere at Callisto (compared to its neighbors Ganymede and Europa) could imply that direct surface sputtering is less important whereas atmospheric sputtering is more relevant by comparison for the long-term evolution of the moon.

## 2.2. Charged Particle Environment and Magnetospheric Interaction

Understanding the physics of Callisto's atmosphere is impossible without studying the interaction of the moon with its space environment inside Jupiter's magnetosphere. Callisto is exposed to the most variable thermal plasma and energetic particle environment among the four Galilean moons: Kivelson et al. (2004) provided a summary table with environment parameters at all Galilean satellites that are generally consistent with plasma moments estimated from more recent analyses (Bagenal, Adriani, et al., 2017; Bagenal, Dougherty, et al., 2017; Bodisch et al., 2017; Dougherty et al., 2017; Kim et al., 2020). Kivelson et al. (2004) indicated, for instance, that the charge density in the thermal plasma upstream of Callisto may change by up to a factor of 70, while at Io, Europa and Ganymede this variability range is 6–20 times weaker. Callisto's orbital distance and location within the magnetosphere are key factors determining the dynamics of the moon's space environment. All four Galilean moons are subject to periodic variations in their ambient particle environment as the Jovian magnetodisk wobbles relative to their orbital plane by  $\pm 10^\circ$  because Jupiter's magnetic dipole axis is offset from its rotation axis by a similar amount. However, the effects of the wobbling at Callisto are stronger compared to the other Galilean moons due to a thinning and an additional hinging of the magnetodisk that begins to develop between 25 and 30  $R_J$  (Khurana, 1992; Khurana et al., 2004). Callisto maps magnetically to a current sheet center distance ranging from 26  $R_J$  when the moon is crossing that center to more than 60  $R_J$  when the magnetic latitude excursion of Callisto is the largest (Liuzzo et al., 2015; Paranicas et al., 2018). Essentially, Callisto changes its magnetic location from the middle to the outer magnetosphere within half a planetary rotation (i.e., within roughly 5 hr). These magnetospheric effects are predicted to be small for particle irradiation surface processes (Paranicas et al., 2018), but must be accounted for by magnetospheric interaction models. On top of the rotational and hinging effects, magnetospheric dynamics further amplify the charged particle environment variations at Callisto's position, as we describe below.

Charged particles in Callisto's space environment can be grouped in three categories: (a) thermal plasma of ions and electrons approximately corotating with the Jovian magnetic field, energies below few keV; (b) suprathermal particles from acceleration processes in the corotating plasma, energies between few keV and hundreds of keV; and finally (c) high-energy particles with a broad angular distribution, reaching up to about 10 MeV in the case of electrons or several 10 MeV/nucleon in the case of protons and heavier ions. Categories 2 and 3 are sometimes combined under the description “energetic particles.”

The thermal plasma environment at Callisto's orbit has been sampled by most spacecraft that visited Jupiter, including Juno, which is currently orbiting the planet (Bagenal, Adriani, et al., 2017; Bagenal, Dougherty, et al., 2017; McComas et al., 2017). Galileo crossed Callisto's orbit more than 60 times (Bagenal et al., 2016) but its plasma instrumentation (Frank et al., 1992) had reduced sensitivity at energies above few keV/e, which made it challenging to resolve the Maxwellian distribution peaks of the thermal ion populations dominated by oxygen and sulfur corotating with velocities  $>200 \text{ km s}^{-1}$  (Bodisch et al., 2017; Dougherty et al., 2017; Waldrop

et al., 2015). Therefore, data from Juno and the Voyager 1 and 2 spacecraft provide the most comprehensive plasma observations at Callisto's orbit (Bagenal, Adriani, et al., 2017; Bagenal, Dougherty, et al., 2017; Bodisch et al., 2017; Dougherty et al., 2017; Huscher et al., 2021; Kim et al., 2020). The thermal plasma is approximately corotating with velocities ranging between 200 and 300 km s<sup>-1</sup> to radial distances of roughly 20 R<sub>J</sub>. At larger radial distances from Jupiter (i.e., roughly from the orbit of Callisto), the ion flow speed starts dropping below corotation speed (Kim et al., 2020). The survey of plasma moments indicates that even when Callisto crosses the center of the Jovian plasma sheet, it is exposed to a highly variable environment (Kim et al., 2020). Part of the variability can be attributed to local time-dependent flows, as inferred from energetic particle measurements of anisotropy (Krupp et al., 2001; Waldrop et al., 2015). The plasma measurements on Juno also allowed to separate the two dominant ion species in the plasma, O<sup>+</sup> and S<sup>2+</sup> to obtain ion density ratios as a function of radial distance (Kim et al., 2020). Taken together, S<sup>2+</sup> and O<sup>+</sup> contribute to ~60% of the total charge density of ~0.3 cm<sup>-3</sup>, with protons, O<sup>2+</sup>, S<sup>+</sup>, and S<sup>3+</sup> having also nonnegligible contributions (Kim et al., 2020). Trace ions, such as sodium, are also present at detectable concentrations. The plasma disk is concentrated around Jupiter's centrifugal equator with a thickness of ±3R<sub>J</sub> on average at distances between 15 and 50 R<sub>J</sub>, as measured by the 1/e decrease in density of electrons and heavy ions (Huscher et al., 2021). The ion kinetic temperatures range from 1 to 10 keV, depending on the species, suggesting that thermal plasma can be an important surface sputtering agent for Callisto (Vorburger et al., 2019). Far from the plasma sheet center, protons tend to become the dominant plasma species, but densities drop faster (by factors of 3–5) than one would expect from the high plasma temperatures observed at lower magnetic latitudes.

The energetic charged particle environment at Callisto (from ~10 keV/nucleon into the MeV range) is similarly dynamic as that of thermal energies. While we currently lack a comprehensive description of this environment in the way that was done for example, for Europa (Bagenal et al., 2016) or Ganymede (Paranicas et al., 1999, 2021), radiation environment models (de Soria-Santacruz et al., 2016; Garrett et al., 2017; Mauk et al., 2004; Sicard-Piet et al., 2011) and the work by Cooper et al. (2001) and Jun et al. (2019) provide empirical descriptions of the average electron and ion spectra at Callisto and the amplitude of their variations. In addition to the empirical models, we know that Callisto's orbital distance is in a region where large-scale charged particle acceleration events take place quite frequently. These have been observed both in energetic heavy ions, up to about 10 MeV/nucleon (Selesnick et al., 2001) and in hundreds of keV to >10 MeV electrons (Yuan et al., 2021). The latter seem to develop more in the dusk and dawn regions of the magnetosphere, between 25 and 30 R<sub>J</sub> from the planet and with a recurrence of less than 1 week. This implies a connection of these global scale injections with the unloading of heavy ion plasma from the magnetosphere through reconnection, which develops over a similar time scale (Kronberg et al., 2007). In terms of partial plasma density, for energies between 50 keV/nucleon and 1 MeV/nucleon, protons are the most abundant species, followed by sulfur and oxygen (Mauk et al., 2004). At higher MeV energies, up to about 10 MeV/nucleon the abundance of energetic carbon ions, with a solar wind origin, becomes comparable to that of sulfur (Cohen et al., 2001). The average shape of energetic electron spectra (10 keV to >10 MeV) can be roughly described with a function reminiscent of a double power law, becoming steeper above a cutoff energy which for Callisto is at about 5 MeV (Kollmann et al., 2018). Over smaller spatial scales, magnetospheric interchange injections, which may expose a moon to extreme fluxes of suprathermal ions and electrons for short periods (minutes), do occur at Callisto's distance, but at a much lower rate compared to the inner Galilean moons (Dumont et al., 2014; Mauk et al., 1999).

In summary, Callisto orbits in an environment exposing it to a high level of particle irradiation, leading among other things to intense surface sputtering. The energetic ion populations alone account for a plasma beta (ratio of particle to magnetic pressure) of  $\beta \sim 10$  (Mauk et al., 2004). This suggests that the configuration's of Callisto's magnetospheric interaction will be dominated by the plasma dynamics and to a lesser extent by properties of the magnetic field. Finally, the environment of Callisto favors a magnetospheric interaction in the transonic regime (magnetosonic Mach number near unity; Kivelson et al., 2004), similar to Rhea at Saturn (Roussos et al., 2008). Given the extreme variability of Callisto's ambient environment it is not unlikely that the moon becomes occasionally exposed to a supersonic flow.

Besides measuring the space environment, the Galileo spacecraft performed seven close Callisto flybys from which mostly magnetic field and ionospheric electron density measurements have been analyzed. Magnetic field signatures reveal the presence of an inductive response by the moon, but it remains debated on whether this response comes from a subsurface ocean (Zimmer et al., 2000), the moon's asymmetric ionosphere discussed

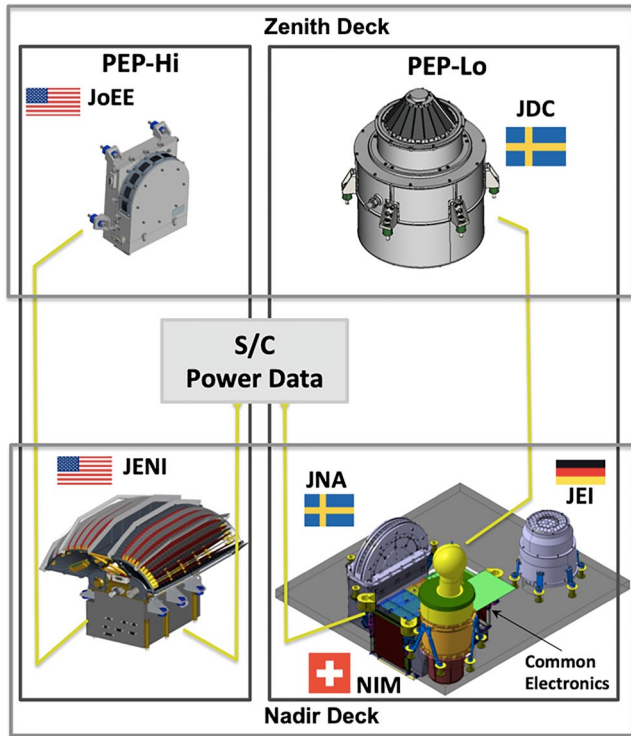


**Figure 1.** Sketch of the six Particle Environment Package (PEP) instruments. Figure adapted from Barabash et al. (2016).

earlier in this section (Cunningham et al., 2015; Hartkorn et al., 2017; Kliore et al., 2002) or a combination of both (Seufert, 2012; Lindkvist et al., 2015; Liuzzo et al., 2015, 2016). The low signal-to-noise ratio of Galileo's plasma instrumentation (Frank et al., 1992) at Callisto's distance is one of the primary reasons that close flyby plasma interaction signatures have not been reported. The same applies to energetic particle observations during Callisto flybys. With the exception of a brief report of field-aligned >10 keV electron beams during the C3 flyby (Mauk & Saur, 2007), when Galileo was passing through Callisto's geometric plasma wake, energetic particle observations from the mission's close flybys remain largely unpublished. These beams may have a similar origin as similar features observed at Io (Mauk et al., 2001; Williams et al., 1996; Williams & Thorne, 2003). On the other hand, Mauk and Saur (2007) suggest that the variability of the energetic particle environment at Callisto is so large that it is very challenging to distinguish in situ interaction features: the C3 flyby electron beams may actually have originated in Jupiter's ambient environment, coincidentally observed during the moon's wake crossing by Galileo.

Expectations about the local plasma and energetic particle interactions of Callisto originate mainly from simulation studies. Many of these studies agree that at least a local ionosphere is necessary to explain the large electron number densities observed near the moon, as well as aspects of magnetic field interaction signatures (Lindkvist et al., 2015; Liuzzo et al., 2015). Liuzzo et al. (2016, 2017) have also shown that besides the variability of plasma density, plasma temperature, and ion composition upstream of Callisto, it is also important to establish the full properties of the plasma velocity vector: radial flow components at Callisto's distance can be nonnegligible and they may impact the inversions for the conductivity, thickness, and depth of the moon's potential subsurface ocean. Callisto's ionosphere is also predicted to

drive a significant magnetic field pile-up and plasma flow deflection around the moon, strong enough to limit precipitation of thermal plasma on the surface and the efficiency on surface sputtering and chemical alterations of Callisto's surface ices. This shielding may change considerably based on the location of the moon with respect to the center of Jupiter's current sheet, with the maximum shielding predicted to occur at intermediate magnetic latitudes, since the induced magnetic dipole increases in strength with magnetic latitude while the density of the ionosphere decreases (Liuzzo et al., 2019a, 2019b; Vorburger et al., 2019). Precipitation patterns of energetic particles may differ significantly from those of low-energy plasma (Liuzzo et al., 2019a, 2019b), offering additional ways to constrain the global configuration of Callisto's magnetospheric interaction region.

### 3. Mission Timeline and PEP Instruments

JUICE contains a full suite of instruments to investigate the space environment, the atmosphere, the surface, and the interior of Jupiter's icy moons (Grasset et al., 2013). In this study, we focus on the possibilities provided by the Particle Environment Package (PEP) for Callisto science. Other JUICE instruments that will contribute to plasma, ionosphere, and atmosphere measurements are the Submillimeter Wave Instrument (SWI; Hartogh et al., 2013), the JMAG magnetometer (Dougherty, 2013), the radio and plasma wave instrument RPWI (Cecconi et al., 2015), the VIS-NIR spectrometer MAJIS (Piccioni & Langevin, 2013; Plainaki et al., 2020), and the RADEM radiation monitor (Desorgher et al., 2015).

#### 3.1. The Particle Environment Package (PEP)

PEP consists of six different instruments (Barabash et al., 2016; Hussmann et al., 2014), which are mounted on the zenith and the nadir deck of the JUICE spacecraft (see Figure 1). The two instruments measuring high-energy particles are addressed as PEP-Hi with US-led instrument teams; the four PEP instruments measuring thermal

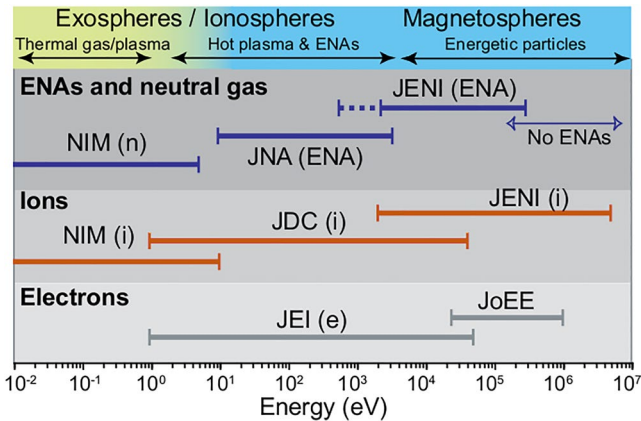


**Figure 2.** Energy ranges and target species covered with the six Particle Environment Package (PEP) instruments. The letters “e,” “i,” and “n” designate electrons, ions, and thermal neutrals, respectively; the dashed line for Jovian Energetic Neutrals and Ions (JENI) between 0.5 and 2 keV indicates the low-energy limit for Energetic Neutral Atoms (ENAs) subject to calibration results. Figure taken from Hussmann et al. (2014).

or low-energy particles are summarized as PEP-Lo with European-led instrument teams. Figure 2 illustrates the energy ranges and target species of the six instruments.

With its six instruments PEP will measure all types of particles relevant for the atmosphere and space environment surrounding Callisto: thermal neutrals, ENAs, ions, and electrons (Barabash et al., 2016). Thermal neutrals (and also ions) will be measured with the neutral mass spectrometer Neutral Gas and Ion Mass (NIM) (see Section 3.1.1). To characterize the charged particle environment around Callisto, PEP will measure energetic electrons 25 keV–1 MeV with JoEE (see Section 3.1.4), thermal and suprathermal electrons from 1 eV to 50 keV energy with JEI (Section 3.1.3), thermal ions and plasma ions at energies 1 eV–41 keV with JDC (Section 3.1.2), and energetic ions between 0.5 keV and 5 MeV with JENI (see Section 3.1.6). The plasma instruments offer mass resolution capability to discern different ion species. PEP is equipped with two instruments capable of imaging ENAs: JNA can image low-energy ENAs between 10 eV and 3 keV (Section 3.1.5), whereas JENI is sensitive to high-energy ENAs from 0.5 to 300 keV. Both of them are mounted on the nadir side of the spacecraft, which will usually be pointed toward Callisto during a flyby. The capability of PEP instruments to measure particles of different polarity (e.g., electrons and ions or ions and ENAs) allows for a better spatial coverage of all species, opportunities for cross-calibration, and for contingency.

### 3.1.1. Neutral Gas and Ion Mass Spectrometer

NIM is a compact time-of-flight mass spectrometer with a reflectron, measuring neutrals and ions either via an open source or a closed source using an antechamber. The advantage of the antechamber is the much wider field-of-view and the better signal-to-noise ratio due to a pressure increase. The potential disadvantage is that the signal will show the thermalized particles that may potentially have been altered upon contact with the antechamber surface even though the coating is chemically inert. NIM and particularly its detector are shielded against the harsh radiation environment around Jupiter to reduce background signals in the detector and to protect NIM electronics against the harsh radiation environment around Jupiter. Calibration of the NIM flight model demonstrated that the scientific requirements (mass range  $m/Z$  of at least 1–650, mass resolution  $m/\Delta m$  of at least 750, and an instantaneous dynamic range of almost six decades in density) are met (Föhn et al., 2021).

### 3.1.2. Jovian Plasma Dynamics and Composition (JDC)

JDC is a plasma spectrometer using a reflectron and a reflecting surface to measure ions (primary goal) and electrons between 1 eV–41 keV. Instantaneous 3D-distributions of positive and negative plasma ions can be obtained, and the charge states of ions can be constrained. The highest mass resolution available is  $m/\Delta m \sim 20$ .

### 3.1.3. Jovian Electrons and Ions (JEI)

JEI is a spectrometer measuring instantaneous 3D-distributions of plasma electrons (primary goal) and ions between 1 eV–50 keV energy with a rather high  $\Delta E/E = 4.9\%$  energy resolution. Both JEI and JDC fields-of-view cover one hemisphere.

### 3.1.4. Jovian Energetic Electrons (JoEE)

JoEE is an ultralightweight energetic electron instrument built on the basis of the Galileo energetic particle detector technique. JoEE measures instantaneous pitch-angle distributions and spectra, with an energy range of 25 keV–1 MeV. The primary target are electrons, but ions can be measured as well.

### 3.1.5. Jovian Neutrals Analyzer (JNA)

JNA images low-energy ENAs (energy range 10 eV–3 keV, also separating between hydrogen and heavier ENAs) based on the ENA imager SARA on the lunar Chandrayaan-1 mission (Barabash et al., 2009). JNA can also measure ions if the high-voltage deflection at the entrance is switched off. The science goals of JNA are to image the backscattered and sputtered surface products from the icy moons of Jupiter, as well as imaging the plasma distributions surrounding the moons.

### 3.1.6. Jovian Energetic Neutrals and Ions (JENI)

JENI is the combined energetic ion and ENA camera based on ENA instruments for the Cassini, IMAGE and Juno missions (Krimigis et al., 2004; Mitchell et al., 2004). JENI allows for global ENA imaging of magnetospheres of the icy moons and neutral gas tori. It is sensitive to ions and electrons from roughly 0.5 keV–5 MeV energy. When a high-voltage deflection is activated to deflect charged particles at the entrance, JENI images high-energy ENAs from roughly 0.5–300 keV energy.

## 3.2. The JUICE Trajectory

The baseline trajectory for JUICE as of November 2021 is 15010a or CRema 5.0 (see ESA project site [www.cosmos.esa.int/web/spice/spice-for-juice](http://www.cosmos.esa.int/web/spice/spice-for-juice) including online displays, ESA SPICE Service, 2022) with several launch date options in 2023 under investigation. The Jupiter orbit insertion will follow in 2031 at the earliest. Potential changes in the trajectory details with respect to the current baseline would not alter the logic of the observational strategy of PEP presented hereafter.

The baseline trajectory foresees 21 Callisto flybys. Out of those, 12 flybys will have closest approaches at 500 km altitude or below, with the minimum flyby altitude at 200 km. The spacecraft speed with respect to the moon and its neutral atmosphere will range between 3 and 6 km s<sup>-1</sup>. The solar zenith angle during closest approach will cover almost the full range from 10° to 170°. These numbers are summarized in Table 1. The 21 flybys can be categorized in terms of plasma configuration into 12 polar, 5 upstream, and 3 downstream flybys (see Figure 3) plus one flank flyby, which fits to neither of the three other categories. Flybys intersecting the flux tube of Callisto around closest approach are listed as polar flyby, upstream flybys have a closest approach upstream of Callisto's trailing hemisphere or sample the ambient magnetospheric environment around closest approach, and flybys crossing the plasma corotation wake behind Callisto's leading hemisphere are categorized as downstream flyby. Keep in mind that due to the tidal locking, the same part of Callisto's surface is always exposed to the wake or upstream plasma flow.

If we consider all 21 flybys in the Jupiter-Sun-Orbit reference frame (see Figure 4), we notice that 15 of the 21 flybys have similar solar longitudes  $\approx 120^\circ$  when Callisto's inner trailing edge is illuminated. These 15 flybys will allow for studying, under the same illumination conditions, the dependencies of Callisto's plasma interaction and atmospheric/ionospheric state from variations in the ambient magnetospheric environment, controlled primarily from Callisto's absolute magnetic latitude (ranging between 2 and 9.5 deg) and time. The remaining six flybys will be crucial to establish the impact of different illumination conditions with respect to the direction of the plasma corotation flow.

Figure 5 shows the JUICE ground tracks on Callisto's surface itself: polar and equatorial regions will be covered. For the purposes of this study, the position of JUICE with respect to the surface is mostly relevant to investigate the three-dimensional structure of the neutral atmosphere and the ENAs or backscattered ions from Callisto's surface, the emission efficiency of which may depend on the diverging surface properties, such as the surface composition, as indicated by similar studies at the Earth's moon (Vorburger et al., 2013). A general list of regions of interest on Callisto's surface for all JUICE instruments and a more thorough discussion about the implications for all remote sensing instruments can be found in the recently published study by Stephan et al. (2021).

**Table 1**

Overview of All 21 Callisto Flybys for the New Baseline JUICE Trajectory, CA = Closest Approach, SZA = Solar Zenith Angle

| Flyby | CA Date                           | CA Altitude (km) | Magnetic Latitude (deg) | Magnetospheric Local time (h) | CA SZA (deg) | Flyby type                                  |
|-------|-----------------------------------|------------------|-------------------------|-------------------------------|--------------|---------------------------------------------|
| 1     | 21 Jun 2032 00:37:41.808          | 3559.6           | -8.30                   | 00:28                         | 103.7        | Downstream, equatorial                      |
| 2     | 29 July 2032 01:49:27.324         | 4437.5           | -3.23                   | 07:03                         | 143.5        | Upstream, equatorial                        |
| 3     | 14 August 2032 18:13:54.987       | 1132.1           | -6.05                   | 06:52                         | 151.7        | Upstream, equatorial                        |
| 4     | 10 September 2032<br>19:24:44.847 | 200.1            | -8.51                   | 21:36                         | 127.0        | Polar, South                                |
| 5     | 27 September 2032<br>11:59:26.081 | 200.0            | 2.94                    | 21:32                         | 99.5         | Polar, South                                |
| 6     | 14 October 2032 04:28:19.156      | 200.0            | 5.47                    | 21:24                         | 121.8        | Polar, South                                |
| 7     | 30 October 2032 20:53:06.906      | 200.0            | -9.26                   | 21:17                         | 125.4        | Polar, South                                |
| 8     | 16 November 2032 13:16:07.918     | 200.0            | 5.45                    | 21:13                         | 127.3        | Polar, South                                |
| 9     | 3 December 2032 05:36:32.439      | 1219.0           | 4.34                    | 21:05                         | 163.8        | Downstream,<br>south polar to<br>equatorial |
| 10    | 24 February 2033 16:07:59.753     | 2071.2           | 9.28                    | 20:35                         | 29.9         | Upstream,<br>equatorial                     |
| 11    | 13 March 2033 08:31:07.776        | 1162.0           | -2.01                   | 20:31                         | 34.1         | Upstream,<br>equatorial                     |
| 12    | 10 May 2033 16:08:56.330          | 313.0            | 2.93                    | 17:00                         | 101.2        | Polar, North                                |
| 13    | 4 June 2033 18:37:57.246          | 200.0            | 9.81                    | 19:56                         | 88.7         | Polar, North                                |
| 14    | 21 June 2033 11:01:19.078         | 200.0            | -5.27                   | 19:53                         | 70.7         | Polar, North                                |
| 15    | 8 July 2033 03:23:27.891          | 200.0            | -3.10                   | 19:44                         | 75.7         | Polar, North                                |
| 16    | 24 July 2033 19:45:47.991         | 200.0            | 9.66                    | 19:37                         | 80.7         | Polar, North                                |
| 17    | 10 August 2033 12:13:43.858       | 200.0            | -6.62                   | 19:34                         | 47.7         | Polar, North                                |
| 18    | 1 November 2033 22:59:42.823      | 315.9            | 4.31                    | 19:01                         | 60.2         | Polar, North                                |
| 19    | 15 February 2034 00:07:42.889     | 643.0            | 7.73                    | 01:32                         | 118.6        | Upstream, equatorial                        |
| 20    | 1 May 2034 22:25:05.048           | 3073.4           | 9.32                    | 14:18                         | 106.9        | Downstream, equatorial                      |
| 21    | 24 June 2034 05:14:43.895         | 6623.7           | -6.90                   | 18:26                         | 75.9         | Flanks                                      |

Note. CA, Closest Approach; SZA, Solar Zenith Angle.

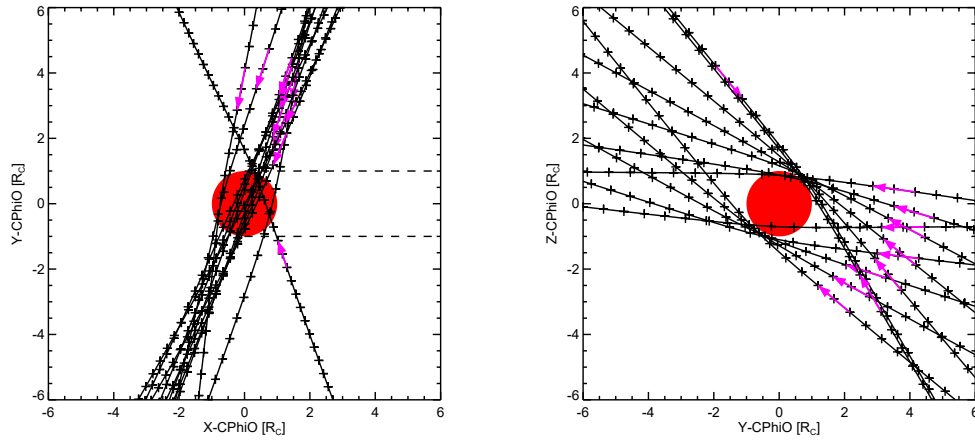
## 4. Science Goals and Opportunities for PEP Observations

The science questions related to Callisto to be answered by PEP measurements are twofold (see Section 1). (A) What are the chemical composition and the three-dimensional distribution of Callisto's atmosphere and ionosphere? and (B) How can Callisto's space environment be characterized and how is it affected by Callisto? Sections 4.1 and 4.2 cover observations of the neutral atmosphere and neutral torus pertaining to the first question, Section 4.3 covers ENA imaging, which is relevant to both questions, and Section 4.4 addresses the charged particle environment central for the second question.

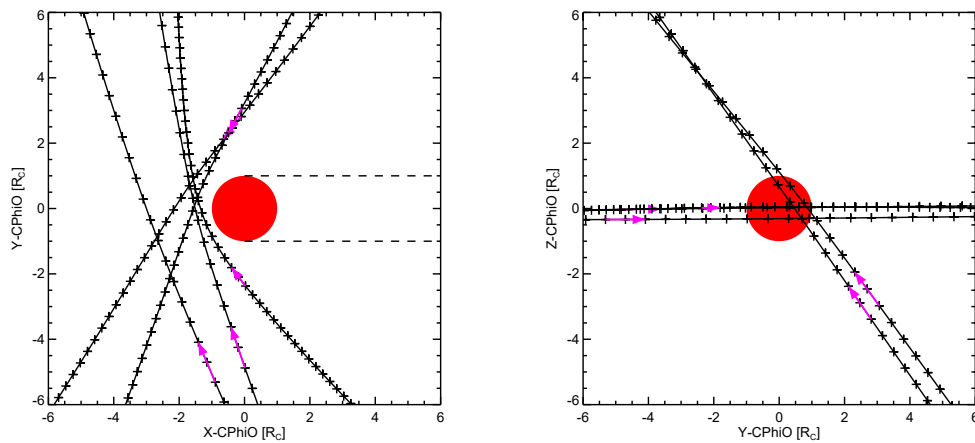
### 4.1. The Neutral Atmosphere

JUICE will revolutionize our knowledge of Callisto's neutral atmosphere. Up to this date, only CO<sub>2</sub> has directly been observed in Callisto's atmosphere (Carlson, 1999). Compare this state of knowledge to the mass spectrum predicted by Vorburger et al. (2015) to be measured with NIM at closest approach of 200 km altitude in Figure 6. For this figure, Callisto's surface was assumed to consist of either ice, the composition of which resembles the oxidizing state of the subnebula, or silicates, the composition of which resembles CI chondrites. The NIM

POLAR FLYBYS



UPSTREAM FLYBYS



DOWNSTREAM FLYBYS

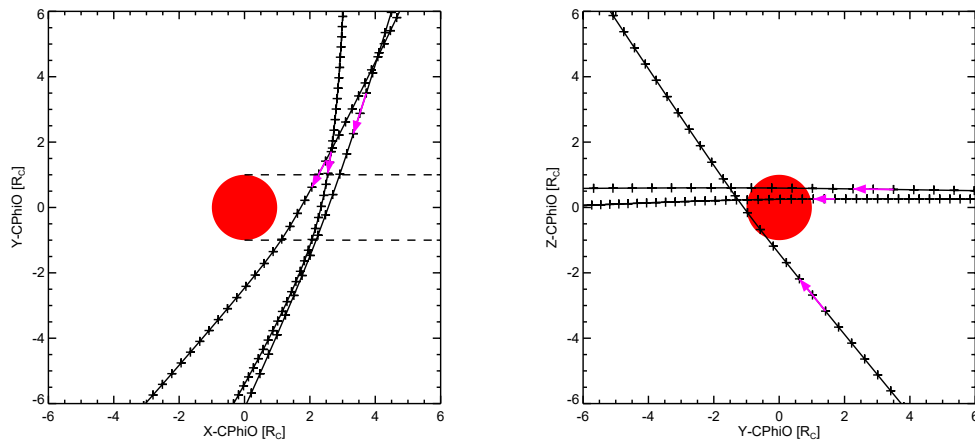


**Figure 3.** The Callisto flybys categorized in terms of plasma configuration in 12 polar (top), 5 upstream (middle), and 3 downstream (bottom panel) flybys, plotted in the  $xy$ -plane (left column) and the  $yz$ -plane (right column) of the Corotation-Jupiter reference frame. In this reference system, the local plasma corotation direction points to  $+X$ , Jupiter is at  $+Y$ , and  $+Z$  closes the right-handed system. The position of Callisto's plasma wake is indicated in the  $xy$ -plane, the pink arrows indicate the spacecraft direction.

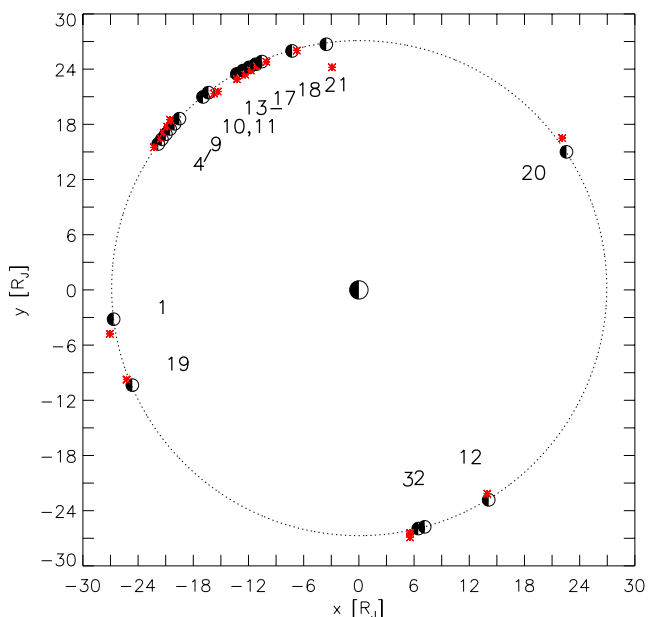


**Figure 4.** All 21 Callisto flybys in the  $xy$ -plane of the Jupiter-Sun-Orbit reference frame in units of Jupiter radii. The Callisto positions are depicted as black and white semi-circles with the latter pointing toward the Sun direction in  $+x$  axis, the red asterisks denote the closest approach of Jupiter ICy moons Explorer (JUICE) for each of the 21 flybys with respect to Callisto.

measurements at close approach will thus reveal dozens of new atmospheric species and hence allow us to infer chemical properties of Callisto's surface.

The default observation strategy with NIM for all Callisto flybys will be to start NIM observations 12 hr before closest approach or at least  $10^5$  km away from Callisto to get the full spatial distribution of the most extended neutral species  $H_2$ , H, and O, which are also relevant for ENA images (see Section 4.3). Then, as JUICE gets closer to Callisto and particle densities increase in general, the temporal resolution of mass spectra will be increased from 100 to 10 s or 5 s (0.2 Hz) at closest approach. This time resolution corresponds—at a flyby relative velocity of typically  $5 \text{ km s}^{-1}$ —to a spatial resolution of roughly 25 km, that is, 0.01 Callisto radii. This is sufficient to resolve possible three-dimensional structures of the Callistoan atmosphere, such as day-night differences (compare the solid, dashed, and dotted curves in Figure 7). For instance, comparing the density profiles measured during upstream flybys 10 and 11 when the trailing hemisphere is illuminated with the upstream flybys 2 and 3 when the trailing hemisphere is on the night-side will allow us to disentangle day-night effects from irradiation effects on Callisto's atmosphere.

One general restriction will affect NIM measurements during flybys: measurements with an unblocked NIM field-of-view will usually only be possible during the inbound phase of a moon flyby. During the outbound leg the Nadir deck of the spacecraft (where NIM is situated) will usually still be pointed toward the moon center to allow for imaging of the the moon surface and limb with remote sensing instruments. As a consequence, the local ram direction of the neutral gas will usually be directed at the spacecraft side opposite

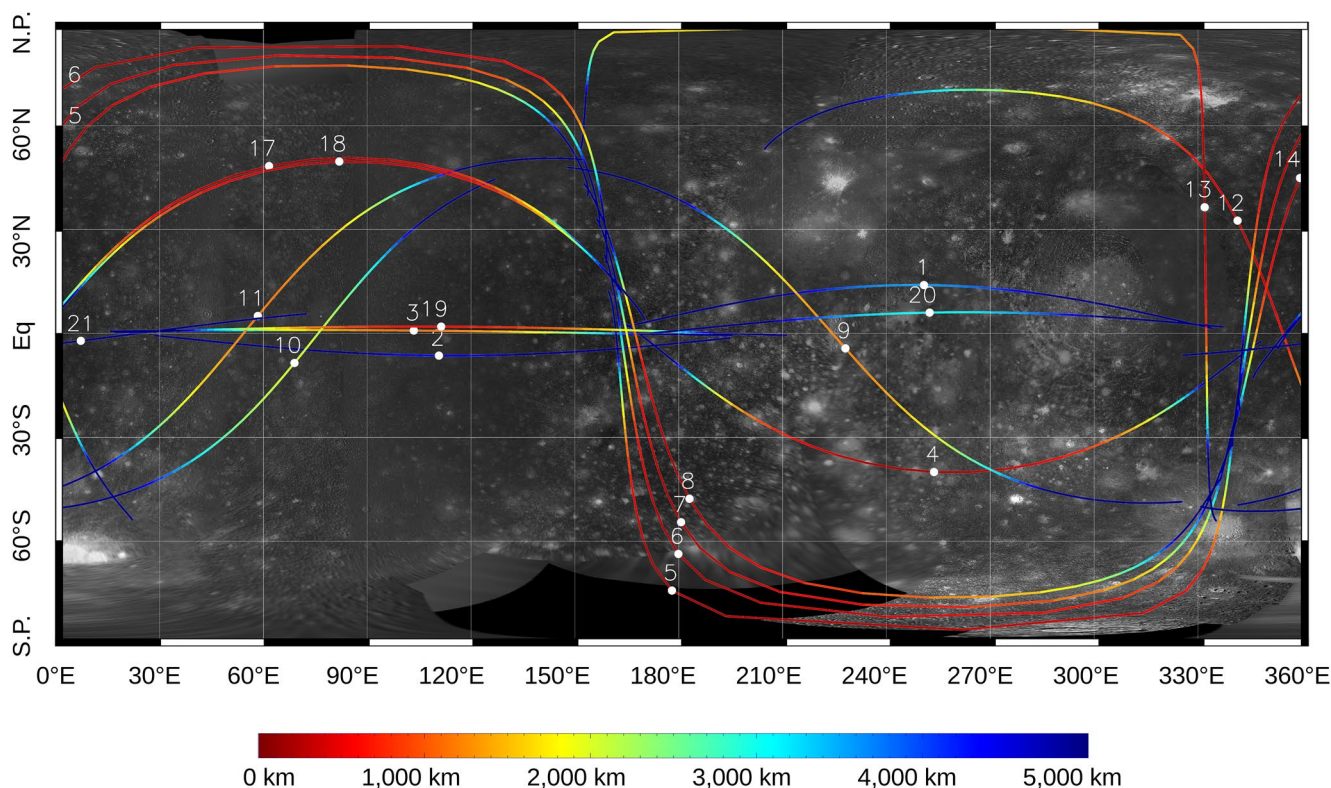


**Figure 5.** Coverage of Callisto's surface for all 21 The Jupiter ICy moons Explorer (JUICE) flybys from 2032 to 2034 (chronologically ordered from 1 to 21), showing the spacecraft ground track every 60 s as a function of altitude. Image created with the software provided by Seignovert et al. (2020-2021).



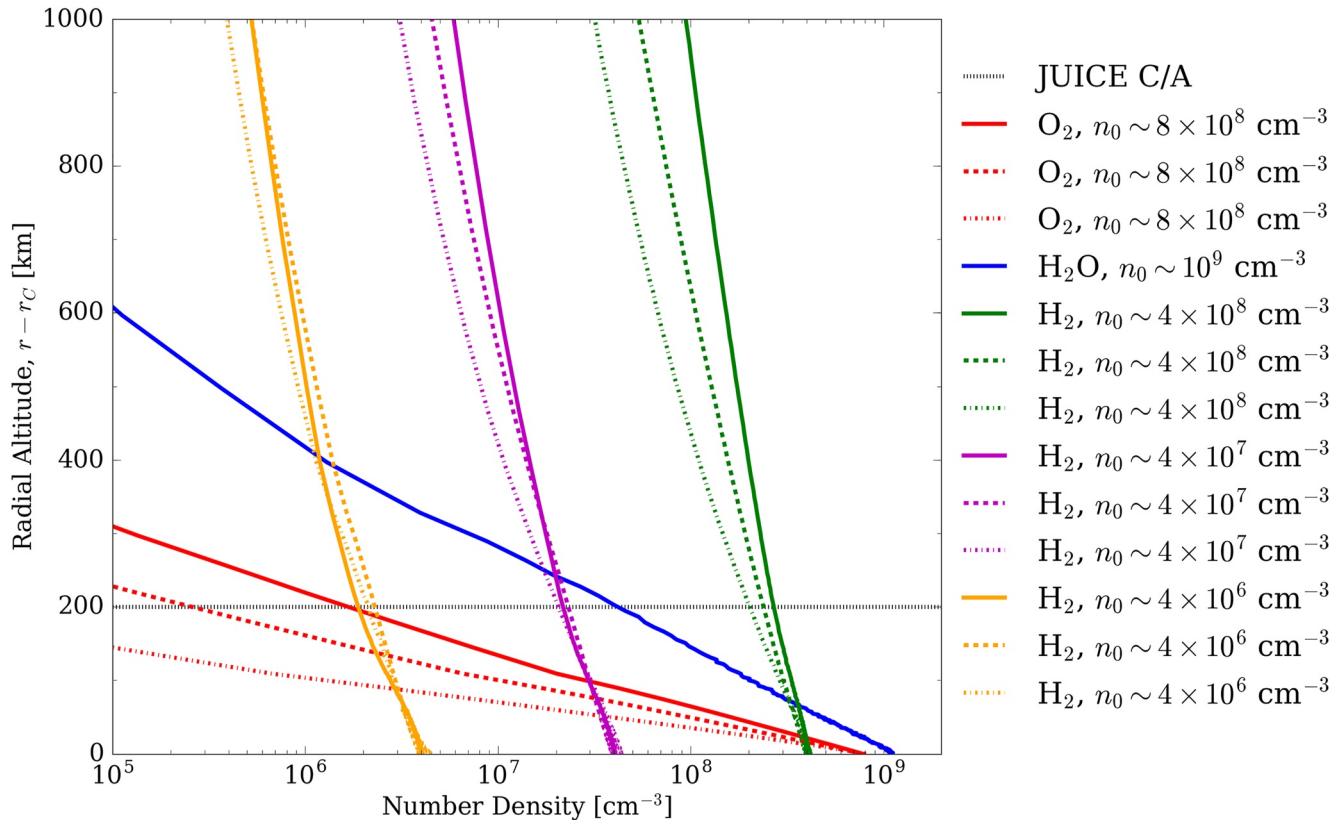


**Figure 7.** Predicted height profiles (Carberry Mogan et al., 2021) of densities for sublimated H<sub>2</sub>O (blue) and radiolytically produced O<sub>2</sub> (red) and H<sub>2</sub> (green, magenta, orange) with surface densities ( $n_0$ ) of  $\sim 10^9$  cm<sup>-3</sup>,  $\sim 8 \times 10^8$  cm<sup>-3</sup>, and  $\sim 4 \times 10^{6-8}$  cm<sup>-3</sup>, respectively, at Callisto for various solar zenith angles (solid lines: 0°, dashed lines: 90°, dotted lines: 180°).

(e.g., radiolysis and sputtering) can be much lower, the H<sub>2</sub> lifetime is much longer than that of the other icy Galilean satellites. Since the torus density roughly scales with the escape rate (e.g., Johnson, 1990), the detection of an H<sub>2</sub> torus would help constrain the surface source rate as well as provide insight into local responses to other magnetospheric processes. To interpret H<sub>2</sub> observations, predictions at eastern and western elongation from 2D models (Carberry Mogan et al., 2021) or predictions from 3D models (Vorburger et al., 2019) could be used.

An important criterion to discuss the neutral torus is the Hill radius of Callisto, which has a radius of 20.8 Callisto radii. Neutral H<sub>2</sub> (or other neutral species) encountered at a larger distance from the moon along the orbit can be attributed to the neutral torus. If we assume for the sake of simplicity only a neutral tail and no persistent neutral torus, that is, the neutrals escaping from Callisto are completely lost within one Callisto orbit due to ionization (in reality, the H<sub>2</sub> lifetimes are much longer than one Callisto orbit, see Table 2 in Carberry Mogan et al. (2021)), the expected H<sub>2</sub> neutral density trailing close behind Callisto (20–100  $R_C$ , one Callisto radius  $R_C = 2,410$  km) would still calculate to  $n_{H_2} = F_{H_2}/v_C \approx 10^3$  cm<sup>-3</sup> with Callisto's orbital speed  $v_C = 8.2$  km s<sup>-1</sup> and the maximum thermal H<sub>2</sub> escape flux of  $F_{H_2} = 6 \times 10^8$  cm<sup>-2</sup> s<sup>-1</sup> estimated by Liang et al. (2005). The H<sub>2</sub> escape fluxes of  $10^9$  to several  $10^{11}$  cm<sup>-2</sup> s<sup>-1</sup> derived by Carberry Mogan et al. (2020) and Carberry Mogan et al. (2021) (the reason for the difference in escape fluxes can be explained by Liang et al. (2005) assuming H<sub>2</sub> only a photochemical product whereas Carberry Mogan et al. (2020) and Carberry Mogan et al. (2021) assume H<sub>2</sub> is a radiolytic product in steady state) would result in a correspondingly higher H<sub>2</sub> density trailing Callisto. Such neutral densities are orders of magnitude above the NIM detection threshold of 1 cm<sup>-3</sup> for 5–100 s of integration time (Föhn et al., 2021).

If NIM detects indeed sizable H<sub>2</sub> densities escaping from Callisto in the first flybys, NIM will also be operated during certain crossings of the moon's orbit far ( $> 10R_C$ ) away from Callisto itself to search for an extended neutral torus. The same applies if, for example, enhanced H<sub>2</sub><sup>+</sup> (or other ion concentrations) are detected at the magnetic distance of Callisto during regular magnetospheric surveys with PEP/JDC. In addition or as an alternative to in

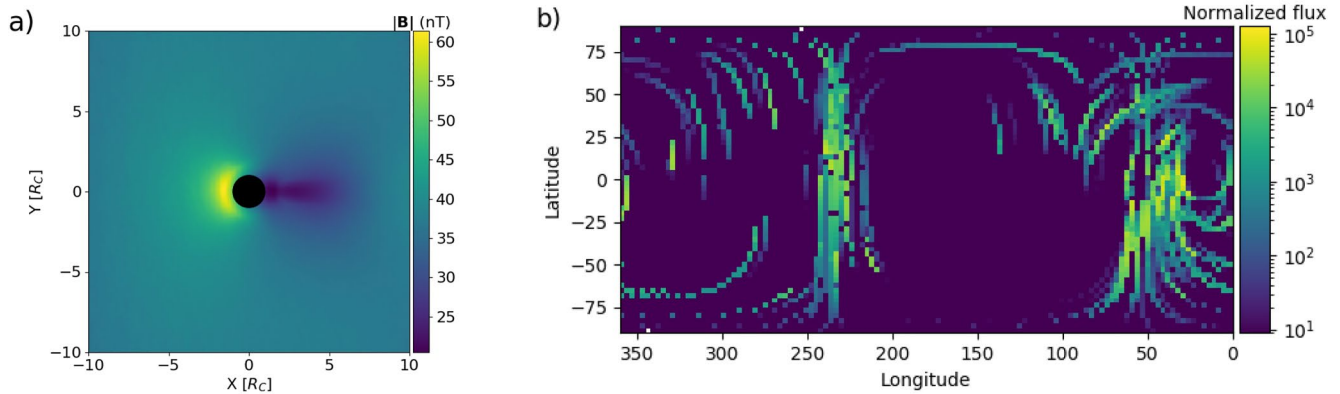


**Figure 8.** (a) Magnetic field magnitude near Callisto in a plane through the center of the moon, containing the upstream flow direction (plasma flows in positive  $x$  direction) and the magnetospheric background field (along  $-y$ ). The structure of the magnetic field was calculated with the AIKEF hybrid model (Liuzzo et al., 2015). The field piles up at Callisto's ramside, while a depletion region is formed in the downstream hemisphere. (b) Energetic Neutral Atom (ENA) flux normalized to an arbitrary background value, through a concentric spherical shell of radius  $3R_C$  (integrated over all ENA energies for a parent ion energy of 30 keV). The horizontal and vertical axes display West longitude and latitude on this sphere, respectively.

situ detection with NIM, the neutral torus could also be characterized via the toroidal interactions of  $H_2$  with the local plasma, producing  $H_2^+$  ions and ENA emissions and by measuring the ion pitch-angle distributions with JENI, similar as it has been done for the Io and Europa tori (see following Sections 4.4 and 4.3). Energetic ions bounce continuously through the torus and are therefore very sensitive (Kollmann et al., 2016; Lagg et al., 1998). A newly ionized  $H_2$  atom maps to magnetic distances ranging from 25 to more than  $60 R_J$  (depending on the place of ionization and the magnetic latitude) because the magnetodisk wobble is very large at Callisto. That would spread the  $H_2^+$  rapidly, reducing  $H_2^+$  fluxes from Callisto. In analogy, high  $H_2^+$  densities are measured in Saturn's magnetosphere, but it is difficult to trace them back to a specific moon (Rhea, Titan?) due to their broad distribution (Felici et al., 2018). This implies for PEP measurements: if a diffuse  $H_2^+$  distribution is found spread out in the Jovian magnetosphere, not collocated with one of the moon orbits, it is important to establish if Callisto is a potential source of neutral and ionized  $H_2$ .

### 4.3. Imaging Energetic Neutral Atoms

ENAs can be used as a means to study the neutral atmosphere and its interaction with the ambient plasma and energetic particle populations. ENAs are the product of a suprathermal or energetic ion exchanging its charge with an ambient neutral particle in the atmosphere of Callisto, or they can originate as reflected and neutralized ions from the surface in analogy to the processes observed at Earth's moon (Allegrini et al., 2013; Futaana et al., 2012; Vorburger et al., 2013; Wieser et al., 2009). The result of a charge exchange between an energetic ion and an ambient neutral atom are a thermal ion and an ENA. The latter will leave the place of its creation on a straight trajectory with the energy of the parent ion, no longer impeded by any magnetic or electric fields. Imaging such ENA emissions thus allows for remote sensing of the neutrals surrounding Callisto and their interaction with charged particles. As detailed in Section 3.1, JNA and JENI will cover the full ENA energy range of interest from 10 eV to 300 keV.

Near Callisto, ENAs are mainly produced by two processes. (a) The charge exchange of the parent ions (the corotational flow and the high-energy particles in the magnetosphere) by the exospheric neutrals and (b) the surface-plasma interaction.

As already known from Saturn's moon Titan (Kabanovic et al., 2018; Wulms et al., 2010), the dynamics of the parent ions and hence, the resulting ENA emission morphology, are strongly affected by the perturbations of the electromagnetic fields near the moon. At Titan, the modeled ENA emission maxima for uniform and draped fields were found to be located in opposite hemispheres (Wulms et al., 2010). The plasma interactions of Callisto and Titan are very similar (see Figure 8): at both moons, the Alfvén Mach number of the upstream flow is on the order of  $M_A \approx 1$  (Kivelson et al., 2004). Besides, the gyroradii of corotating magnetospheric and ionospheric pick-up ions exceed the size of the obstacle to the flow by up to an order of magnitude, thereby imposing pronounced

asymmetries on the flow deflection and associated magnetic draping pattern (Liuzzo et al., 2015, 2016; Simon et al., 2015). In analogy to Titan, any reasonable model of ENA emissions at Callisto should therefore take into account the influence of the draped electromagnetic fields on the trajectories of the incoming energetic parent ions.

So far, ENA emissions around Callisto have never been modeled. To give an impression of the hydrogen ENA emission morphology expected at Callisto in this overview study, we have combined the draped electromagnetic fields calculated by the AIKEF hybrid model (Liuzzo et al., 2015, 2016, 2017, 2018, 2019a, 2019b) with the ENA emission model originally developed for Titan (Kabanovic et al., 2018). We consider the upstream conditions from setup # three of Liuzzo et al. (2019b): Callisto is exposed to a flow of magnetospheric  $O^+$  ions with a number density of  $0.58 \text{ cm}^{-3}$ , approaching the moon along the corotation direction at a relative velocity of 192 km/s. The moon is assumed to be located in Jupiter's *northern* magnetodisk lobe, that is, the magnetospheric background field points away from the giant planet and the field magnitude is set to 33.6 nT. This combination of upstream parameters yields an Alfvén Mach number of  $M_A = 0.8$  and a magnetosonic Mach number of  $M_{MS} = 0.6$ . Our model setup considers only the plasma interaction with Callisto's partially ionized gas envelope, but does not take into account any induced fields from the moon's interior or ionosphere. An induced field would add additional complexity to the magnetic field near the moon (Liuzzo et al., 2016, 2019a, 2019b). These effects will be investigated separately in a more extended follow-up study.

To model the generation of ENAs, a planar “starting grid” with a resolution of  $0.2R_C$  is placed at a distance of  $6R_E$  upstream of the moon. From the nodes of this grid, magnetospheric protons with an initial energy of 30 keV are launched toward Callisto. The protons' equations of motion in the draped electromagnetic fields are solved with a fourth-order Runge-Kutta scheme. Protons entering Callisto's exosphere can generate ENAs through charge-exchange reactions with the neutral gas. Each modeled proton can produce multiple ENAs, and each charge-exchange reaction goes along with a decrease in the numerical “weight” of the proton (corresponding to the number of real magnetospheric ions it represents). The velocity vector of a newly generated ENA is identical to that of the parent proton at the moment of the charge-exchange reaction. For details of the procedure, the reader is referred to Section of Kabanovic et al. (2018). Callisto's exosphere is modeled as spherically symmetric, consisting of  $O_2$  and  $CO_2$  with the neutral gas densities described by a barometric law and parameters from Table 3 of Liuzzo et al. (2015). The addition of neutral  $H_2O$  close to the surface and  $H_2$  with its large-scale height could be important, too, and should be considered in future ENA studies at Callisto.

Due to limitations on the field of view, a spacecraft instrument can capture only a fraction of the ENA population generated by the moon-magnetosphere interaction during one specific flyby. Thus, multiple flybys along different trajectories and under similar upstream conditions are required to fully understand the ENA emission morphology at Callisto. To obtain an idea of the global ENA emission pattern independent of the viewing geometry, we recorded the modeled ENA flux through a concentric spherical shell of radius  $3R_C$ . The right panel in Figure 8 displays the ENA emission morphology obtained from this model. With a scale height way below 100 km, Callisto's atmosphere is clearly exceeded by the gyroradii of the impinging parent ions. As a result, a highly nonuniform ENA emission pattern is formed near the moon: ENA emissions are by several orders of magnitude more intense in Callisto's Jupiter-facing hemisphere (around  $0^\circ$  West longitude) than in its Jupiter-averted hemisphere (around  $180^\circ$  West longitude). This hemispheric dichotomy in the emission pattern is caused by the enhanced protection from parent ion impacts onto Callisto's Jupiter-averted hemisphere, rendered by the asymmetric shape of the moon's magnetic pile-up region (Liuzzo et al., 2015). The region of enhanced magnetic field at Callisto's ramside is stretched away from Jupiter, following the outer flank of the moon's cycloidal pick-up tail. ENA emissions are observable in both Callisto's ramside ( $180^\circ$ – $360^\circ$  W) and wakeside ( $0^\circ$ – $180^\circ$  W) hemispheres. In addition, the nonuniform fields tend to “focus” the incident parent ions into several “preferred” regions of the moon's atmosphere, thereby generating multiple ray-like fine structures in the ENA emissions through the detector sphere (see Figure 8). A follow-up publication solely dedicated to ENA emissions will investigate the origin of these signatures in more detail.

The surface-plasma interaction is another source of the ENAs as seen on our Moon (Futaana et al., 2006, 2012; Wieser et al., 2009). The sputtering and backscattering processes are two main sources of ENA production. In the Jovian magnetic field, due to the high-energy penetrating fluxes, the sputtering process is expected to be a dominant source (Wieser et al., 2016). The sputtered ENA emission from Ganymede was simulated (Pontoni

et al., 2022), showing that the sputtered ENAs from the surface can be detected with JNA. Thus, PEP can map the ion precipitation onto Ganymede (Pontoni et al., 2022). The same mapping should also be possible for Callisto.

#### 4.4. The Charged Particle Environment of Callisto

To study Callisto's neutral atmosphere, we need to consider its coupling to the ionosphere and to the Jovian plasma environment in which the moon is immersed. The PEP instruments will be able to measure all species and energy ranges relevant for these studies (see Section 3.1). The issue raised by Mauk and Saur (2007) about the large intrinsic variability of the energetic particle environment at Callisto must be tackled with an improved observational basis: JUICE will offer us many more flybys with dedicated instrumentation for plasma and high-energy particles to obtain a more comprehensive picture of the particle environment compared with the seven Galileo flybys. To optimize the science return, several PEP instruments and the JMAG magnetometer will always be operational to measure magnetic fields, electrons, and the different ion species including energy spectra over the entire JUICE trajectory far away from and close to Callisto to disentangle Jovian variability from the features induced by Callisto.

Understanding the way that Callisto interacts with Jupiter's magnetosphere is a multicomponent problem, which requires that we disentangle its neutral gas envelope (Section 4.1) from the variable ambient magnetospheric particle environment and the moon's ionosphere and plasma interaction signatures. Separating these contributions would allow to set tighter constraints on the properties of Callisto's subsurface conducting ocean layer and to understand the moon as a source of plasma for Jupiter's magnetosphere (Liuzzo et al., 2018).

Many of the science goals guiding the plasma measurements are also important for the study of the atmosphere. The average properties of the plasma upstream Callisto is an important parameter. The spatial and temporal scales on which the environment changes have implications on the coupling and the particle input to the atmosphere. The precipitating fluxes of ions and electrons at different energies must be characterized in order to derive the altitude depended energy deposition and the ionization rates. Charged particles reaching the surface may lead to sputtering and radiolysis and is another source of material released to the atmosphere. Neutral particles in the atmosphere can be ionized and energized reach escape velocities. The size of the atmospheric escape determines if Callisto is an important source of plasma for Jupiter's magnetosphere.

In many regards, the ionosphere is the interface between the plasma environment and the neutral atmosphere. Understanding the coupling between the neutral atmosphere, the ionosphere and the plasma environment is one of the keys to understanding both the entire system and the individual components. To achieve this goal observations of the ionospheric properties (density, temperature, scale height, composition, conductivity) are crucial. These properties may vary depending on the state of the neutral atmosphere and on the upstream conditions, which will reveal the interaction between the layers. Callisto's location in the Jovian magnetosphere and the solar UV input will most likely strongly affect the ionosphere and coupling to the atmosphere (Hartkorn et al., 2017; Kliore et al., 2002; Seufert, 2012).

## 5. Plans and Recommendations

The state of knowledge on Callisto's atmosphere and space environment combined with the prospects offered by PEP lead us to the following recommendations for scientific studies in this decade and for the PEP operations:

### 5.1. Scientific Studies on Callisto's Atmosphere and Its Space Environment

Further efforts are needed to develop and compare 3D models of the neutral atmosphere and ionosphere, interactions with magnetosphere, for example, atmospheric sputtering and energy deposition, and ionospheric shielding of magnetosphere. This includes studies of spatial asymmetries and temporal variations in preparation to the observations enabled by JUICE. One of the outcomes of these model efforts should be narrower constraints on atmospheric source and loss rates. There is currently no consensus for source rates and surface processes (sputtering, radiolysis, sublimation) for several key species such as H<sub>2</sub>O, O<sub>2</sub>, H<sub>2</sub>, and CO<sub>2</sub> (Carberry Mogan et al., 2020, 2021; Liang et al., 2005; Vorburger et al., 2015), and it is difficult to make any direct correlations to those of Europa and Ganymede.

Models of Callisto's ambient plasma and energetic charged particle environments should extend the empirical environment descriptions by adding information on the particles' angular distribution, (energetic) ion composition, and charge state from Galileo and Juno, where this is available. The models should also link these observational constraints with information on the physical processes that drive Jupiter's magnetospheric configuration at Callisto's distance in order to constrain the predictions for the environment's dynamical variations and characteristic time scales. Until the arrival of JUICE, existing plasma and energetic particle observations from Galileo flybys, which remain largely unpublished until now, should be analyzed or reassessed.

The influence of porosity and the reactions in Callisto's regolith, the relevance of thermal inertia and local cold trapping (Spencer, 1987) need to be studied in more detail regarding their impacts on the atmospheric volatiles, in particular for water. Also compare the findings to other icy satellites of Jupiter and Saturn (e.g., by Leblanc et al. (2017) at Ganymede and Oza et al. (2019) at Europa). For this task, also laboratory experiments should be undertaken (in analogy to, e.g., Fountain and West, 1970; Gundlach & Blum, 2012; Sakatani et al., 2017).

ENA model predictions for Callisto should be extended to various plasma conditions and to ENA species other than hydrogen. ENA emissions generated by parent ion species other than hydrogen are apparently negligible at Titan (Kabanovic et al., 2018; Wulms et al., 2010) but this should be reassessed for the case of the Galilean moons before the arrival of JUICE. Including the putative Callisto neutral torus in ENA models would also allow to optimize PEP operations planning.

## 5.2. Recommendations for PEP Operations

Because Callisto's atmosphere and ionosphere must be observed at various combinations of illumination versus leading-trailing hemisphere to disentangle different sources of the atmosphere, the six flybys at a solar longitude far from the common one around 120° (flyby numbers 1, 2, 3, 12, 19, 20 in Figure 4) are particularly important.

During each of the 21 Callisto flybys, simultaneous electron, ion, and neutrals data will be recorded on the way to closest approach. After the closest approach when JUICE moves away from the moon, no useful NIM measurements can be obtained because the incoming neutral gas will be blocked from the instrument entrance by the spacecraft itself. On the other hand, plasma, and ENA observations will continue to distances far away from Callisto to obtain a farther vantage point for ENA emissions and to cover additional plasma regimes and boundaries. Ten seconds will be the shortest measurement interval for PEP data acquisition except for electron data (~1 s).

Neutral gas measurements with NIM must be started—at a slow cadence—12 hr before closest approach of every Callisto flyby, which corresponds to a distance from Callisto of  $(1-2) \times 10^5$  km or 40–80  $R_c$ . The reason for this wide range is to put observational constraints on the putative neutral torus and the extended H corona of Callisto. To detect the Callisto torus (Section 4.2), also remote observations with the ENA imagers and opportunities to measure neutral densities at the Jovian-centric distance of Callisto when Callisto is opposite of Jupiter may be needed. These measurements will also prove crucial to better constrain atmospheric source and escape rates of light species from Callisto (see Section 4.1).

Trajectories that cross plasma wake and interaction regions are generally rewarding for in situ plasma measurements. Therefore, from the perspective of plasma measurements, the understanding of the current system established in the moon's interaction region and for the determination of the atmospheric loss rates in the form of pick-up ions, more than the three downstream flybys would be preferable. Wakeside flybys could be used to measure the magnetospheric electron and ion flux (with its ambient levels measured before and after the flyby) that has been lost due to its precipitation on Callisto's surface or atmosphere. ENA imaging during those downstream flybys could help disentangle atmospheric and surface losses.

Upstream flybys are also ideal for linking ENA imaging observations with in situ observations of the Callisto's ambient environment and its variations, especially if the environment can vary on time scales comparable to or shorter than the flyby duration: for downstream or polar flybys, such variations may be masked when JUICE is crossing the moon's interaction region. The lowest altitude upstream flybys (flyby numbers 11, 19) may also cross into the magnetic pile-up region (Figure 8) and provide direct measurements of the precipitating flux by JDC, JEI, JENI, and JoEE in connection with NIM measurements of the atmosphere and ENA images by JNA and JENI (which can be simultaneously operated in ENA and ion mode). Notably, flyby 19 occurs with the upstream

hemisphere of Callisto largely in darkness (i.e., sputtering dominates), whereas flyby 11 has the upstream hemisphere sunlit, where sublimation would be most important.

The nightside flybys in general will be very interesting for atmosphere models because they will inform us if the sublimated atmosphere on Callisto collapses while in shadow. Flybys will span the full range of possible magnetic latitudes from  $-10^\circ$  to  $10^\circ$  (see Table 1) with the Jovian current sheet expected close to  $0^\circ$ . This will allow us to see if the ENA emissions change in dependence of the current sheet position.

For a better handle on ENA emissions, measuring the distribution functions of the parent ions upstream of Callisto is crucial. For Callisto, just one single energy spectrogram of ion flux has been published by Cooper et al. (2001), averaged over a time of several hours. This is too long an average to say anything about Callisto's local environment. Moreover, there are no reliable data of the pitch-angle distribution of the parent ions upstream of Callisto. So far, this pitch-angle distribution has to be assumed to be isotropic.

Europa Clipper, with a planned launch for October 2024 and a Jupiter Orbit insertion in 2030, will also perform several Callisto flybys at roughly the same time as JUICE, but the scientific priorities of Europa Clipper are concentrated on Europa (<https://europa.nasa.gov>).

## 6. Conclusions

The prospects offered by PEP on JUICE for studies of Callisto's atmosphere and its space environment are promising. This study has collected recommendations for PEP operations and science preparations related to Callisto's atmosphere.

The baseline trajectory 5.0 for a JUICE launch in September 2021 foresees 21 Callisto flybys in total, with closest approaches both on the day side and the night side. This is a good variety for Callisto surface coverage; for atmosphere and plasma science investigations more downstream flybys and more flybys at solar longitudes outside the  $90^\circ$ – $180^\circ$  quadrant would be welcome.

The 13 flybys with a closest approach below 1,000 km will be crucial to detect heavy neutrals and ions. On the other hand, neutral measurements should be started at distances  $>40R_C$  away from Callisto to better constrain the putative neutral torus and the extended hydrogen corona.

Fortunately, the background rates due to radiation levels in Jovian magnetosphere at Callisto will be much lower than near Europa or Ganymede.

Recommendations for scientific studies for the present decade are to improve models of Callisto's atmosphere in combination with its space environment, improve ENA model predictions, analyze existing plasma data from Galileo and to perform laboratory experiments on Callisto surface analogs in analogy to, for example, Galli et al. (2016) and Pommerol et al. (2019).

We are looking forward to the JUICE mission and PEP observations as they will enable accurate and localized measurements of the particle environment, the neutral atmosphere (including spatial distribution of major species), and surface composition thus revolutionizing our understanding of the outermost of the four Galilean moons.

## Data Availability Statement

The data and model outputs reanalyzed for this study are available under the sources referenced in the text, that is, the atmosphere model data are available through Vorburger et al. (2015, 2019) and Carberry Mogan et al. (2020, 2021), the AIKEF model data are available through Liuzzo et al. (2015). The software tool used to create the moon coverage image and other JUICE related plots is available through Seignovert et al. (2020–2021), the JUICE Operational SPICE Kernel Data Set is available via <https://doi.org/10.5270/esa-ybmj68p> (ESA SPICE Service, 2022).

## Acknowledgments

L. L. acknowledges support from NASA Solar System Workings Grant No. 80NSSC21K0152. S. R. C. M., O. J. T., and R. E. J. acknowledge support from NASA Goddard Space Flight Center's Solar System Exploration Division Grant No. 80NSSC20M0193. The work of Sven Simon and Tyler Tippens was supported by NASA's Solar System Workings program (Grant No. 80NSSC22K0097).

## References

- Allegrini, F., Dayeh, M., Desai, M., Funsten, H., Fuselier, S., Janzen, P., & Wurz, P. (2013). Lunar energetic neutral atom (ENA) spectra measured by the interstellar boundary explorer (IBEX). *Planetary and Space Science*, 85, 232–242. <https://doi.org/10.1016/j.pss.2013.06.014>
- Anderson, J. D., Lau, E. L., Sjogren, W. L., Schubert, G., & Moore, W. B. (1997). Gravitational evidence for an undifferentiated Callisto. *Nature*, 387(6630), 264. <https://doi.org/10.1038/387264a0>
- Bagenal, F., Adriani, A., Allegrini, F., Bolton, S. J., Bonfond, B., Bunce, E. J., et al. (2017). Magnetospheric science objectives of the Juno mission. *Space Science Reviews*, 213, 219–287. <https://doi.org/10.1007/s11214-014-0036-8>
- Bagenal, F., Dougherty, L. P., Bodisch, K. M., Richardson, J. D., & Belcher, J. M. (2017). Survey of voyager plasma science ions at Jupiter: 1. Analysis method. *Journal of Geophysical Research: Space Physics*, 122, 8241–8256. <https://doi.org/10.1002/2016JA023797>
- Bagenal, F., Wilson, R. J., Siler, S., Paterson, W. R., & Kurth, W. S. (2016). Survey of Galileo plasma observations in Jupiter's plasma sheet. *Journal of Geophysical Research: Planets*, 121, 871–894. <https://doi.org/10.1002/2016JE005009>
- Barabash, S., Bhardwaj, A., Wieser, M., Sridharan, R., Kurian, T., Varier, S., & Wurz, P. (2009). Investigation of the solar wind-moon interaction onboard Chandrayaan-1 mission with the sara experiment. *Current Science*, 96, 526–532.
- Barabash, S., Brandt, P., Wurz, P., & PEP Team. (2016). Particle environment package (PEP) for the ESA JUICE mission. In *3rd International Workshop on instrumentation for planetary missions* (Vol. 3). Retrieved from <https://www.hou.usra.edu/meetings/ipm2016/pdf/4079.pdf>
- Bodish, K. M., Dougherty, L. P., & Bagenal, F. (2017). Survey of voyager plasma science ions at Jupiter: 3. Protons and minor ions. *Journal of Geophysical Research: Space Physics*, 122, 8277–8294. <https://doi.org/10.1002/2017JA024148>
- Carberry Mogan, S. R., Tucker, O. J., Johnson, R. E., Sreenivasan, K. R., & Kumar, S. (2020). The influence of collisions and thermal escape in Callisto's atmosphere. *Icarus*, 352, 113932. <https://doi.org/10.1016/j.icarus.2020.113932>
- Carberry Mogan, S. R., Tucker, O. J., Johnson, R. E., Vorburger, A., Galli, A., Marchand, B., et al. (2021). A tenuous, collisional atmosphere on Callisto. *Icarus*, 368, 114597. <https://doi.org/10.1016/j.icarus.2021.114597>
- Carlson, R. W. (1999). A tenuous carbon dioxide atmosphere on Jupiter's moon Callisto. *Science*, 283(5403), 820–821. <https://doi.org/10.1126/science.283.5403.820>
- Cecconi, B., Kasaba, Y., Bergman, J. E. S., Zarka, P., Lamy, L., Hess, S. L. G., & Rothkaehl, H. (2015). *JUICE/RPWI/JENRAGE: A low frequency radio imager at Jupiter*. Paper Presented at *European Planetary Science Congress, Nantes, France*. Retrieved from <https://www.meetingorganizer.copernicus.org/EPSC2015/EPSC2015-919.pdf>
- Celletti, A., Karampotsiou, E., Lhotka, C., Pucacco, G., & Volpi, M. (2021). Laplace-like resonances with tidal effects. *Astronomy & Astrophysics*, 655, A94. <https://doi.org/10.1051/0004-6361/202141311>
- Cohen, C. M. S., Stone, E. C., & Selesnick, R. S. (2001). Energetic ion observations in the middle Jovian magnetosphere. *Journal of Geophysical Research*, 106(A12), 29871–29882. <https://doi.org/10.1029/2001JA000008>
- Cooper, J. F., Johnson, R. E., Mauk, B. H., Garrett, H. B., & Gehrels, N. (2001). Energetic ion and electron irradiation of the icy Galilean satellites. *Icarus*, 149(1), 133–159. <https://doi.org/10.1006/icar.2000.6498>
- Cunningham, N. J., Spencer, J. R., Feldman, P. D., Strobel, D. F., France, K., & Osterman, S. N. (2015). Detection of callisto's oxygen atmosphere with the Hubble space telescope. *Icarus*, 254, 178–189. <https://doi.org/10.1016/j.icarus.2015.03.021>
- de Soria-Santacruz, M., Garrett, H. B., Evans, R. W., Jun, I., Kim, W., Paranicas, C., & Drozdov, A. (2016). An empirical model of the high-energy electron environment at Jupiter. *Journal of Geophysical Research: Space Physics*, 121, 9732–9743. <https://doi.org/10.1002/2016JA023059>
- Desorgher, L., Hajdas, W., Goncalves, P., Pinto, C., Marques, A., Chastellain, F., & Meier, D. (2015). *Development of radiation hard electron monitor RADEM for ESA JUICE mission*. Paper Presented at *European Geophysics Union General Assembly, Vienna, Austria*. Retrieved from <https://meetingorganizer.copernicus.org/EGU2015/EGU2015-11661.pdf>
- Dougherty, L. P., Bodisch, K. M., & Bagenal, F. (2017). Survey of voyager plasma science ions at Jupiter: 2. Heavy ions. *Journal of Geophysical Research*, 122, 8257–8276. <https://doi.org/10.1002/2017JA024053>
- Dougherty, M. K. (2013). *J-MAG: Magnetometer science on the juice mission*. Paper Presented at *European Planetary Science Congress, London, UK*. Retrieved from <https://meetingorganizer.copernicus.org/EPSC2013/EPSC2013-470.pdf>
- Dumont, M., Grodent, D., Radioti, A., Bonfond, B., & Gérard, J. C. (2014). Jupiter's equatorward auroral features: Possible signatures of magnetospheric injections. *Journal of Geophysical Research: Space Physics*, 119, 10068–10077. <https://doi.org/10.1002/2014JA020527>
- ESA SPICE Service. (2022). *Juice operational spice kernel dataset* [Data set]. <https://doi.org/10.5270/esa-ybmj68p>
- Felici, M., Arridge, C. S., Wilson, R. J., Coates, A. J., Thomsen, M., & Reisenfeld, D. (2018). Survey of thermal plasma composition in saturn's magnetosphere using time-of-flight data from Cassini/Caps. *Journal of Geophysical Research: Space Physics*, 123, 6494–6513. <https://doi.org/10.1029/2017JA025085>
- Föhn, M., Galli, A., Vorburger, A., Tulej, M., Lasi, D., Riedo, A., et al. (2021). Description of the ion-optical system of a mass spectrometer for JUPITER's ICy moons Explorer. *IEEE Aerospace Conference*, 50100, 1–14. <https://doi.org/10.1109/AERO50100.2021.9438344>
- Fountain, J. A., & West, E. A. (1970). Thermal conductivity of particulate basalt as a function of density in simulated lunar and martian environments. *Journal of Geophysical Research*, 75(20), 4063–4069. <https://doi.org/10.1029/JB075i020p04063>
- Frank, L., Ackerson, K. L., Lee, J. A., English, M. R., & Pickett, G. L. (1992). The plasma instrumentation for the Galileo Mission. *Space Science Reviews*, 60, 283–304. [https://doi.org/10.1007/978-94-011-2512-3\\_11](https://doi.org/10.1007/978-94-011-2512-3_11)
- Futaana, Y., Barabash, S., Holmström, M., & Bhardwaj, A. (2006). Low energy neutral atoms imaging of the moon. *Planetary and Space Science*, 54, 132–143. <https://doi.org/10.1016/j.pss.2005.10.010>
- Futaana, Y., Barabash, S., Wieser, M., Holmström, M., Lue, C., Wurz, P., & Asamura, K. (2012). Empirical energy spectra of neutralized solar wind protons from the lunar regolith. *Journal of Geophysical Research*, 117, E05005. <https://doi.org/10.1029/2011JE004019>
- Galli, A., Vorburger, A., Pommerol, A., Wurz, P., Jost, B., Poch, O., & Thomas, N. (2016). Surface charging of thick porous water ice layers relevant for ion sputtering experiments. *Planetary and Space Science*, 126, 63–71. <https://doi.org/10.1016/j.pss.2016.03.016>
- Garrett, H., Jun, I., Evans, R., Kim, W., & Brinza, D. (2017). The latest Jovian-trapped proton and heavy ion models. *IEEE Transactions on Nuclear Science*, 64(11), 2802–2813. <https://doi.org/10.1109/TNS.2017.2755618>
- Grasset, O., Dougherty, M. K., Coustenis, A., Bunce, E. J., Erd, C., Titov, D., & Van Hoolst, T. (2013). JUPITER ICy moons Explorer (JUICE): An ESA mission to orbit Ganymede and to characterise the Jupiter system. *Planetary and Space Science*, 78, 1–21. <https://doi.org/10.1016/j.pss.2012.12.002>
- Gundlach, B., & Blum, J. (2012). Outgassing of icy bodies in the solar system—II: Heat transport in dry, porous surface dust layers. *Icarus*, 219, 618. <https://doi.org/10.1016/j.icarus.2012.03.013>
- Gurnett, D. A., Kurth, W. S., Roux, A., & Bolton, S. J. (1997). Absence of a magnetic-field signature in plasma-wave observations at Callisto. *Nature*, 387(6630), 261–262. <https://doi.org/10.1038/387261a0>

- Hand, K. P., Chyba, C. F., Priscu, J. C., Carlson, R. W., & Neelson, K. H. (2009). Astrobiology and the potential for life on Europa. In R. T., Pappalardo (Ed.), *Europa* (pp. 589–629). University of Arizona.
- Hartkorn, O., Saur, J., & Strobel, D. F. (2017). Structure and density of Callisto's atmosphere from a fluid-kinetic model of its ionosphere: Comparison with Hubble Space Telescope and Galileo observations. *Icarus*, 282, 237–259. <https://doi.org/10.1016/j.icarus.2016.09.020>
- Hartogh, P., Barabash, S., Beaudin, G., Börner, P., Bockelée-Morvan, D., Boogaerts, W., et al. (2013). *The submillimetre wave instrument on JUICE. Paper Presented at European Planetary Science Congress, London, UK*. Retrieved from <https://meetingorganizer.copernicus.org/EPSC2013/EPSC2013-710.pdf>
- Huscher, E., Bagenal, F., Wilson, R. J., Allegrini, F., Ebert, R. W., Valek, P. W., et al. (2021). Survey of Juno observations in Jupiter's plasma disk: Density. *Journal of Geophysical Research: Space Physics*, 126, e2021JA029446. <https://doi.org/10.1029/2021JA029446>
- Hussmann, H., Palumbo, P., Jaumann, R., Dougherty, M., Langevin, Y., Piccioni, G., & Kaspi, Y. (2014). *Juice JUPITER ICY moons Explorer—Exploring the emergence of habitable worlds around gas giants around gas giants* (Definition Study Rep. ESA/SRE 2014, (p. 1). European Space Agency.
- Johnson, R. E. (1990). *Energetic charged-particle interactions with atmospheres and surfaces*. Springer Science & Business Media.
- Johnson, R. E. (2004). The magnetospheric plasma-driven evolution of satellite atmospheres. *The Astrophysical Journal*, 609, L99–L102. <https://doi.org/10.1086/422912>
- Jun, I., Garrett, H. B., Cassidy, T. A., Kim, W., & Dougherty, L. (2019). Updating the Jovian electron plasma environment. *IEEE Transactions on Plasma Science*, 47(8), 3915–3922. <https://doi.org/10.1109/TPS.2019.2901681>
- Kabanovic, S., Feyerabend, M., Simon, S., Meeks, Z., & Wulms, V. (2018). Influence of asymmetries in the magnetic draping pattern at Titan on the emission of energetic neutral atoms. *Planetary and Space Science*, 152, 142–164. <https://doi.org/10.1016/j.pss.2017.12.017>
- Khurana, K. K. (1992). A generalized hinged-magnetodisc model of Jupiter's nightside current sheet. *Journal of Geophysical Research*, 97(A5), 6269–6276. <https://doi.org/10.1029/92JA00169>
- Khurana, K. K., Kivelson, M. G., Russell, C. T., Walker, R. J., & Southwood, D. J. (1997). Absence of an internal magnetic field at Callisto. *Nature*, 387(6630), 262. <https://doi.org/10.1038/387262a0>
- Khurana, K. K., Kivelson, M. G., Stevenson, D. J., Schubert, G., Russell, C. T., Walker, R. J., & Polanskey, C. (1998). Induced magnetic fields as evidence for subsurface oceans in Europa and Callisto. *Nature*, 395(6704), 777. <https://doi.org/10.1038/27394>
- Khurana, K. K., Kivelson, M. G., Vasyliunas, V. M., Krupp, N., Woch, J., Lagg, A., & Kurth, W. S. (2004). The configuration of Jupiter's magnetosphere. In F. Bagenal, T. E. Dowling, & T. E. McKinnon (Eds.), *Jupiter: The planet, satellites and magnetosphere* (pp. 593–616). Cambridge University Press.
- Kim, T. K., Ebert, R. W., Valek, P. W., Allegrini, F., McComas, D. J., Bagenal, F., & Bolton, S. J. (2020). Survey of ion properties in Jupiter's plasma sheet: Juno JADE-I observations. *Journal of Geophysical Research*, 125, e27696. <https://doi.org/10.1029/2019JA027696>
- Kivelson, M. G., Bagenal, F., Kurth, W. S., Neubauer, F. M., Paranicas, C., & Saur, J. (2004). Magnetospheric interactions with satellites. In F. Bagenal & T. E. Dowling (Eds.), *Jupiter: The planet, satellites and magnetosphere* (pp. 513–536). Cambridge University Press.
- Kivelson, M. G., Khurana, K. K., Russell, C. T., Walker, R. J., Warnecke, J., Coroniti, F. V., & Schubert, G. (1996). Discovery of Ganymede's magnetic field by the Galileo spacecraft. *Nature*, 384(6609), 537. <https://doi.org/10.1038/384537a0>
- Kliore, A. J., Anabtawi, A., Herrera, R. G., Asmar, S. W., Nagy, A. F., Hinson, D. P., & Flasar, F. (2002). Ionosphere of Callisto from Galileo radio occultation observations. *Journal of Geophysical Research*, 107(A11), 1407. <https://doi.org/10.1029/2002JA009365>
- Kollmann, P., Paranicas, C., Clark, G., Roussos, E., Lagg, A., & Krupp, N. (2016). The vertical thickness of Jupiter's Europa gas torus from charged particle measurements. *Geophysical Research Letters*, 43, 9425. <https://doi.org/10.1002/2016GL070326>
- Kollmann, P., Roussos, E., Paranicas, C., Woodfield, E. E., Mauk, B. H., Clark, G., & Vandegriff, J. (2018). Electron acceleration to MeV energies at Jupiter and Saturn. *Journal of Geophysical Research: Space Physics*, 123, 9110–9129. <https://doi.org/10.1029/2018JA025665>
- Krimigis, S. M., Mitchell, D. G., Hamilton, D. C., Livi, S., Dandouras, S., Jaskulek, T. P., et al. (2004). Magnetospheric imaging instrument on the Cassini mission to Saturn/Titan. *Space Science Review*, 114, 233–329. <https://doi.org/10.1007/s11214-004-1410-8>
- Kronberg, E. A., Glassmeier, K. H., Woch, J., Krupp, N., Lagg, A., & Dougherty, M. K. (2007). A possible intrinsic mechanism for the quasi-periodic dynamics of the Jovian magnetosphere. *Journal of Geophysical Research*, 112, A05203. <https://doi.org/10.1029/2006JA011994>
- Krupp, N., Lagg, A., Livi, S., Wilken, B., Woch, J., Roelof, E. C., & Williams, D. J. (2001). Global flows of energetic ions in Jupiter's equatorial plane: First-order approximation. *Journal of Geophysical Research*, 106(A11), 26017–26032. <https://doi.org/10.1029/2000JA900138>
- Kuskov, O., & Kronrod, V. (2005). Internal structure of Europa and Callisto. *Icarus*, 177(2), 550–569. <https://doi.org/10.1016/j.icarus.2005.04.014>
- Lagg, A., Krupp, N., Woch, J., Livi, S., Wilken, B., & Williams, D. J. (1998). Determination of the neutral number density in the Io torus from Galileo-EPD measurements. *Geophysical Research Letters*, 25, 4039. <https://doi.org/10.1029/1998GL1900070>
- Leblanc, F., Oza, A. V., Leclercq, L., Schmidt, C., & Cassidy, T. (2017). On the orbital variability of Ganymede's atmosphere. *Icarus*, 293, 185–198. <https://doi.org/10.1016/j.icarus.2017.04.025>
- Liang, M.-C., Lane, B. F., Pappalardo, R. T., Allen, M., & Yung, Y. L. (2005). Atmosphere of Callisto. *Journal of Geophysical Research*, 110, E02003. <https://doi.org/10.1029/2004JE002322>
- Lindkvist, J., Holmström, M., Khurana, K. K., Fatemi, S., & Barabash, S. (2015). Callisto plasma interactions: Hybrid modeling including induction by a subsurface ocean. *Journal of Geophysical Research: Space Physics*, 120, 4877–4889. <https://doi.org/10.1002/2015JA021212>
- Liuzzo, L., Feyerabend, M., Simon, S., & Motschmann, U. (2015). The impact of Callisto's atmosphere on its plasma interaction with the Jovian magnetosphere. *Journal of Geophysical Research: Space Physics*, 120, 9401–9427. <https://doi.org/10.1002/2015JA021792>
- Liuzzo, L., Simon, S., & Feyerabend, M. (2018). Observability of Callisto's inductive signature during the JUPITER ICY moons Explorer mission. *Journal of Geophysical Research: Space Physics*, 123, 9045–9054. <https://doi.org/10.1029/2018JA025951>
- Liuzzo, L., Simon, S., Feyerabend, M., & Motschmann, U. (2016). Disentangling plasma interaction and induction signatures at Callisto: The Galileo C10 flyby. *Journal of Geophysical Research: Space Physics*, 121, 8677–8694. <https://doi.org/10.1002/2016JA023236>
- Liuzzo, L., Simon, S., Feyerabend, M., & Motschmann, U. (2017). Magnetic signatures of plasma interaction and induction at Callisto: The Galileo C21, C22, C23, and C30 flybys. *Journal of Geophysical Research: Space Physics*, 122, 7364–7386. <https://doi.org/10.1002/2017JA024303>
- Liuzzo, L., Simon, S., & Regoli, L. (2019a). Energetic electron dynamics near Callisto. *Planetary and Space Science*, 179, 104726. <https://doi.org/10.1016/j.pss.2019.104726>
- Liuzzo, L., Simon, S., & Regoli, L. (2019b). Energetic ion dynamics near Callisto. *Planetary and Space Science*, 166, 23–53. <https://doi.org/10.1016/j.pss.2018.07.014>
- Lopes, R. M. (2014). Io: The volcanic moon. In *Encyclopedia of the solar system* (pp. 779–792). Elsevier. <https://doi.org/10.1016/b978-0-12-415845-0.00035-9>
- Marconi, M. L. (2007). A kinetic model of Ganymede's atmosphere. *Icarus*, 190(1), 155–174. <https://doi.org/10.1016/j.icarus.2007.02.016>
- Mauk, B. H., Mitchell, D. G., McEntire, R. W., Paranicas, C. P., Roelof, E. C., Williams, D. J., & Lagg, A. (2004). Energetic ion characteristics and neutral gas interactions in Jupiter's magnetosphere. *Journal of Geophysical Research*, 109, A09S12. <https://doi.org/10.1029/2003JA010270>

- Mauk, B. H., & Saur, J. (2007). Equatorial electron beams and auroral structuring at Jupiter. *Journal of Geophysical Research*, *112*, A10221. <https://doi.org/10.1029/2007JA012370>
- Mauk, B. H., Williams, D. J., & Eviatar, A. (2001). Understanding Io's space environment interaction: Recent energetic electron measurements from Galileo. *Journal of Geophysical Research*, *106*(A11), 26195–26208. <https://doi.org/10.1029/2000JA002508>
- Mauk, B. H., Williams, D. J., McEntire, R. W., Khurana, K. K., & Roederer, J. G. (1999). Storm-like dynamics of Jupiter's inner and middle magnetosphere. *Journal of Geophysical Research*, *104*(A10), 22759–22778. <https://doi.org/10.1029/1999JA900097>
- McComas, D. J., Alexander, N., Allegrini, F., Bagenal, F., Beebe, C., Clar, G., et al. (2017). The Jovian auroral distributions experiment (jade) on the Juno mission to Jupiter. *Space Science Reviews*, *213*, 547–643. <https://doi.org/10.1007/s11214-013-9990-9>
- Mitchell, D. G., Jaskulek, S. E., Schlemm, C. E., Keath, E. P., & Thompson, R. E. (2004). High energy neutral atom (HENA) imager for the IMAGE mission. *Space Science Review*, *91*, 67–112.
- Moore, J. M., Asphaug, E., Morrison, D., Spencer, J. R., Chapman, C. R., Bierhaus, B., et al. (1999). Mass movement and landform degradation on the icy Galilean satellites: Results of the Galileo nominal mission. *Icarus*, *140*(2), 294–312. <https://doi.org/10.1006/icar.1999.6132>
- Musotto, S., Varadi, F., Moore, W., & Schubert, G. (2002). Numerical simulations of the orbits of the Galilean satellites. *Icarus*, *159*(2), 500–504. <https://doi.org/10.1006/icar.2002.6939>
- Oza, A. V., Leblanc, F., Johnson, R. E., Schmidt, C., Leclercq, L., Cassidy, T. A., & Chaufray, J.-Y. (2019). Dusk over dawn O<sub>2</sub> asymmetry in Europa's near-surface atmosphere. *Planetary and Space Science*, *167*, 23–32. <https://doi.org/10.1016/j.pss.2019.01.006>
- Paranicas, C., Hibbitts, C. A., Kollmann, P., Ligier, N., Hendrix, A. R., Nordheim, T. A., & Clark, G. (2018). Magnetospheric considerations for solar system ice state. *Icarus*, *302*, 560–564. <https://doi.org/10.1016/j.icarus.2017.12.013>
- Paranicas, C., Paterson, W. R., Cheng, A. F., Mauk, B. H., McEntire, R. W., Frank, L. A., & Williams, D. J. (1999). Energetic particle observations near Ganymede. *Journal of Geophysical Research*, *104*(A8), 17459–17470. <https://doi.org/10.1029/1999JA900199>
- Paranicas, C., Szalay, J. R., Mauk, B. H., Clark, G., Kollmann, P., Haggerty, D. K., & Bolton, S. (2021). Energy spectra near Ganymede from Juno data. *Geophysical Research Letters*, *48*, e93021. <https://doi.org/10.1029/2021GL093021>
- Piccioni, G., & Langevin, Y. (2013). MAJIS (moons and Jupiter imaging spectrometer) for JUICE: Jupiter system objectives. Paper Presented at *European Planetary Science Congress, London, UK*. Retrieved from <https://meetingorganizer.copernicus.org/EPSC2013/EPSC2013-417.pdf>
- Plainaki, C., Sindoni, G., Grassi, D., Cafarelli, L., D'Aversa, E., Massetti, S., & Altieri, F. (2020). Preliminary estimation of the detection possibilities of Ganymede's water vapor environment with MAJIS. *Planetary and Space Science*, *191*, 105004. <https://doi.org/10.1016/j.pss.2020.105004>
- Pommerol, A., Jost, B., Poch, O., Yoldi, Z., Brouet, Y., Gracia-Berná, A., & Thomas, N. (2019). Experimenting with mixtures of water ice and dust as analogues for icy planetary material. *Space Science Reviews*, *215*, 37. <https://doi.org/10.1007/s11214-019-0603-0>
- Pontoni, A., Shimoyama, M., Futaana, Y., Fatemi, S., Poppe, A. R., Wieser, M., & Barabash, S. (2022). Simulations of energetic neutral atom sputtering from Ganymede in preparation for the juice mission. *Journal of Geophysical Research: Space Physics*, *127*, e2021JA029439. <https://doi.org/10.1029/2021JA029439>
- Rambaux, N., Van Hoolst, T., & Karatekin, O. (2011). Librational response of Europa, Ganymede, and Callisto with an ocean for a non-Keplerian orbit. *Astronomy & Astrophysics*, *527*, A118. <https://doi.org/10.1051/0004-6361/201015304>
- Roth, L., Alday, J., Becker, T. M., Ivchenko, N., & Retherford, K. D. (2017). Detection of a hydrogen corona at Callisto. *Journal of Geophysical Research: Planets*, *122*, 1046–1055. <https://doi.org/10.1002/2017JE005294>
- Roussos, E., Müller, J., Simon, S., Bößwetter, A., Motschmann, U., Krupp, N., & Dougherty, M. K. (2008). Plasma and fields in the wake of Rhea: 3-D hybrid simulation and comparison with Cassini data. *Annales Geophysicae*, *26*(3), 619–637. <https://doi.org/10.5194/angeo-26-619-2008>
- Sakatani, N., Ogawa, K., Iijima, Y., Arakawa, M., Honda, R., & Tanaka, S. (2017). Thermal conductivity model for powdered materials under vacuum based on experimental studies. *AIP Advances*, *7*, 015310. <https://doi.org/10.1063/1.4975153>
- Schenk, P. M. (1995). The geology of Callisto. *Journal of Geophysical Research*, *100*(E9), 19023–19040. <https://doi.org/10.1029/95JE01855>
- Seignovert, B., Tobie, G., Robidel, R., Vallat, C., Belgacem, I., & Altobelli, N. (2021). *Python moon-coverage toolbox*. Retrieved from <https://moon-coverage.readthedocs.io>
- Selesnick, R. S., Cohen, C. M. S., & Khurana, K. K. (2001). Energetic ion dynamics in Jupiter's plasma sheet. *Journal of Geophysical Research*, *106*(A9), 18895–18906. <https://doi.org/10.1029/2000JA000242>
- Seufert, M. (2012). *Callisto: Induction signals, atmosphere and plasma interaction*. (Unpublished doctoral dissertation). Universität zu Köln.
- Sicard-Piet, A., Bourdarie, S., & Krupp, N. (2011). Jose: A new Jovian specification environment model. *IEEE Transactions on Nuclear Science*, *58*(3), 923–931. <https://doi.org/10.1109/TNS.2010.2097276>
- Simon, S., Roussos, E., & Paty, C. S. (2015). The interaction between Saturn's moons and their plasma environments. *Physics Reports*, *602*, 1–65. <https://doi.org/10.1016/j.physrep.2015.09.005>
- Smith, B. A., Soderblom, L. A., Beebe, R., Boyce, J., Briggs, G., Carr, M., & Veverka, J. (1979). The Galilean satellites and Jupiter: Voyager 2 imaging science results. *Science*, *206*(4421), 927–950. <https://doi.org/10.1126/science.206.4421.927>
- Smith, B. A., Soderblom, L. A., Johnson, T. V., Ingersoll, A. P., Collins, S. A., Shoemaker, E. M., et al. (1979). The Jupiter system through the eyes of voyager 1. *Science*, *204*(4396), 951–972. <https://doi.org/10.1126/science.204.4396.951>
- Smith, H. T., Mitchell, D. G., Johnson, R. E., Mauk, B. H., & Smith, J. E. (2020). Europa neutral torus confirmation and characterization based on observations and modeling. *The Astrophysical Journal*, *871*, 69.
- Smyth, W. H., & Marconi, M. L. (2006). Europa's atmosphere, gas tori, and magnetospheric implications. *Icarus*, *181*, 510. <https://doi.org/10.1016/j.icarus.2005.10.019>
- Spencer, J. R. (1987). Thermal segregation of water ice on the Galilean satellites. *Icarus*, *69*(2), 297–313. [https://doi.org/10.1016/0019-1035\(87\)90107-2](https://doi.org/10.1016/0019-1035(87)90107-2)
- Spohn, T., & Schubert, G. (2003). Oceans in the icy Galilean satellites of Jupiter? *Icarus*, *161*(2), 456–467. [https://doi.org/10.1016/s0019-1035\(02\)00048-9](https://doi.org/10.1016/s0019-1035(02)00048-9)
- Stephan, K., Hibbitts, C. A., & Jaumann, R. (2020). H<sub>2</sub>O-ice particle size variations across Ganymede's and Callisto's surface. *Icarus*, *337*, 113440. <https://doi.org/10.1016/j.icarus.2019.113440>
- Stephan, K., Roatsch, T., Tosi, F., Matz, K.-D., Kersten, E., Wagner, R., et al. (2021). Regions of interest on Ganymede's and Callisto's surfaces as potential targets for ESA's JUICE mission. *Planetary and Space Science*, *208*, 105324. <https://doi.org/10.1016/j.pss.2021.105324>
- Strobel, D. F., Saur, J., Feldman, P. D., & McGrath, M. A. (2002). Hubble space telescope space telescope imaging spectrograph search for an atmosphere on Callisto: A Jovian unipolar inductor. *The Astrophysical Journal Letters*, *581*(1), L51. <https://doi.org/10.1086/345803>
- Vorbürger, A., Pflieger, M., Lindkvist, J., Holmström, M., Lammer, H., Lichtenegger, H. I. M., & Wurz, P. (2019). 3D-modeling of Callisto's surface sputtered exosphere environment. *Journal of Geophysical Research: Space Physics*, *124*, 7151–7169. <https://doi.org/10.1029/2019JA026610>
- Vorbürger, A., Wurz, P., Barabash, S., Wieser, M., Futaana, Y., Lue, C., & Asamura, K. (2013). Energetic neutral atom imaging of the lunar surface. *Journal of Geophysical Research: Space Physics*, *118*, 3937–3945. <https://doi.org/10.1002/jgra.50337>

- Vorburger, A., Wurz, P., Lammer, H., Barabash, S., & Mousis, O. (2015). Monte-Carlo simulation of Callisto's exosphere. *Icarus*, 262, 14–29. <https://doi.org/10.1016/j.icarus.2015.07.035>
- Waldrop, L. S., Roelof, E. C., & Fritz, T. A. (2015). Three-dimensional convective flows of energetic ions in Jupiter's equatorial magnetosphere. *Journal of Geophysical Research: Space Physics*, 120, 10506–10527. <https://doi.org/10.1002/2015JA021103>
- Wieser, M., Barabash, S., Futaana, Y., Holmström, M., Bhardwaj, A., Sridharan, R., & Asamura, K. (2009). Extremely high reflection of solar wind protons as neutral hydrogen atoms from regolith in space. *Planetary and Space Science*, 57, 2132–2134. <https://doi.org/10.1016/j.pss.2009.09.012>
- Wieser, M., Futaana, Y., Barabash, S., & Wurz, P. (2016). Emission of energetic neutral atoms from water ice under Ganymede surface-like conditions. *Icarus*, 269, 91–97. <https://doi.org/10.1016/j.icarus.2015.12.043>
- Williams, D. J., Mauk, B. H., McEntire, R. E., Roelof, E. C., Armstrong, T. P., Wilken, B., & Lanzerotti, L. J. (1996). Electron beams and ion composition measured at Io and in its torus. *Science*, 274(5286), 401–403. <https://doi.org/10.1126/science.274.5286.401>
- Williams, D. J., & Thorne, R. M. (2003). Energetic particles over Io's polar caps. *Journal of Geophysical Research*, 108(A11), 1397. <https://doi.org/10.1029/2003JA009980>
- Wulms, V., Saur, J., Strobel, D. F., Simon, S., & Mitchell, D. G. (2010). Energetic neutral atoms from Titan: Particle simulations in draped magnetic and electric fields. *Journal of Geophysical Research*, 115, A06310. <https://doi.org/10.1029/2009JA014893>
- Yuan, C., Zuo, Y., Roussos, E., Wei, Y., Hao, Y., Sun, Y., & Krupp, N. (2021). Large-scale episodic enhancements of relativistic electron intensities in Jupiter's radiation belt. *Earth and Planetary Physics*, 5, 314–326. <https://doi.org/10.26464/epp2021037>
- Zimmer, C., Khurana, K. K., & Kivelson, M. G. (2000). Subsurface oceans on Europa and Callisto: Constraints from Galileo magnetometer observations. *Icarus*, 147(2), 329–347. <https://doi.org/10.1006/icar.2000.6456>